SECOND ORDER, LINEAR AND UNCONDITIONALLY ENERGY STABLE SCHEMES FOR A HYDRODYNAMIC MODEL OF SMECTIC-A LIQUID CRYSTALS

RUI CHEN [†] AND XIAOFENG YANG [‡⋆] AND HUI ZHANG [§]

Abstract. In this paper, we consider the numerical approximations for a hydrodynamical model of smectic-A liquid crystals. The model, derived from the variational approach of the modified Oseen-Frank energy, is a highly nonlinear system that couples the incompressible Navier-Stokes equations and a constitutive equation for the layer variable. We develop two linear, second-order time-marching schemes based on the "Invariant Energy Quadratization" method for nonlinear terms in the constitutive equation, the projection method for the Navier-Stokes equations, and some subtle implicit-explicit treatments for the convective and stress terms. Moreover, we prove the well-posedness of the linear system and their unconditionally energy stabilities rigorously. Various numerical experiments are presented to demonstrate the stability and the accuracy of the numerical schemes in simulating the dynamics under shear flow and the magnetic field.

1. Introduction

Liquid crystals (LCs) are one important intermediate phase which exhibits features from both the solid and the fluid state, e.g., it flows like liquids, while at the same time, displays an ordering property like solid. Thus it is often viewed as the fourth state of the matter besides the gas, liquid and solid. There are two main different phases in thermotropic liquid crystals: nematic and smectic. In nematic phases, the rod-like molecules self-align to have a long-range directional order with their long axes roughly parallel. While maintaining long-range directional order, the molecules are free to flow and their center of mass positions are randomly distributed as in a liquid, see [6, 7, 13, 17, 21–24, 43, 50, 66, 71, 74–77, 84]. In smectic phases, the molecules maintain the general orientational order of nematics, but also tend to align themselves in layers or planes. Hence, molecules in this state show a degree of translational order that are not present in the nematic phase. Motion is restricted to within these planes, and separate planes are observed to flow past each other, see [5, 7, 10, 11, 14, 24–26, 30, 39, 43, 48]. Note there are many different smectic phases, all characterized by different types and degrees of positional and orientational order. Here we consider the numerical approximations for the smectic-A phase, where the directions of molecules are perpendicular to the smectic plane, and there is no particular positional order inside the layer.

There is a large quantity of studies on modeling and simulation to investigate the flows of liquid crystal systems. One of the most well-known continuum theories is the Ericksen-Leslie

[†] School of Science, Beijing University of Posts and Telecommunications, Beijing 100876, P.R. China, Email: ruichenbnu@gmail.com.

[‡⋆]Corresponding author, Department of Mathematics, University of South Carolina, Columbia, SC, 29208, USA; Beijing Institute for Scientific and Engineering Computing, Beijing University of Technology, Beijing 100124, China. Email: xfyang@math.sc.edu.

[§]School of Mathematical Sciences, Beijing Normal University, Laboratory of Mathematics and Complex Systems, Ministry of Education, Beijing 100875, P.R. China, Email: hzhang@bnu.edu.cn.

theory [16, 17, 38], where, to describe this anisotropic structure, a dimensionless unit vector, called the *director*, is introduced to represent the direction of preferred orientation of molecules in the neighborhood of any point. The corresponded mathematical model can often be obtained from the energetic variational approach for the phenomenon-logical Oseen-Frank energy, leading to a well-posed nonlinear gradient flow system. The first mathematical model for the smectic-A phase is developed in the pioneering work [13] by de Gennes et. al., where the Oseen-Frank energy is modified by coupling the director field and a complex order parameter that represents the layer structure. Following the model of de Genes et. al., a number of models for smectic phase have been developed and studied during the last two decades, see [1, 7, 10, 14, 24, 30, 43, 52]. In this paper, we consider the numerical approximations for solving a particular hydrodynamics coupled smectic-A model developed by W. E. in [14] since it appears to the minimal model of unknowns, where the director field is assumed to be strictly equal to the gradient of the layer and thus the total free energy is reduced to a simplified version with one order parameter. In addition, rather than imposing non-convex constraint directly on the gradient of the layer variable, we use a commonly used technique in liquid crystal theory to modify the free energy by adding a penalization potential of a Ginzburg-Landau type. Such a term can efficiently relax the unit norm constraint numerically, while, in the meantime, it also introduces a stiffness issue into the system [2, 11, 30, 73, 84], for which certain numerical methods like fully implicit or explicit type methods (cf. [20, 55]), are numerically unstable.

From the numerical point of view, for a stiff PDE system, we expect to establish schemes that can verify the so called "energy stable" property at the discrete level irrespectively of the coarseness of the discretization, namely, the energy stability does not impose any limitations on the time step. In what follows, those algorithms will be called *unconditionally energy stable*. Schemes with this property is specially preferred since it is not only critical for the numerical scheme to capture the correct long time dynamics with large time steps, but also provides sufficient flexibility for dealing with the stiffness issue. However, it is remarkable that, unlike the enormous algorithm developments on the nematic models (cf. [12, 37, 42, 45–47, 57, 85, 87–90]), very few attempts of developing energy stable schemes had been made for smectic models in any form. We notice, for solving the particular smectic-A model of W. E. [14], Guillén et. al. developed a linear, second order scheme in [30], where the nonlinear term induced by the penalization Ginzburg-Landau potential is approximated by a Hermite quadrature formula. This scheme can be regarded as one of the limited efforts in the algorithm designs, however, it is not unconditionally energy stable, i.e., there exists a time step constraint that is dependent on the penalization parameter, so it is not efficient in practice.

Therefore, in this paper, the main purpose is to develop some more efficient and effective numerical schemes for solving the hydrodynamics coupled smectic-A model in [14]. We expect that our developed schemes can own the following three desired properties, i.e., (i) accurate (second order in time); (ii) stable (the unconditional energy dissipation law holds); and (iii) easy to implement and efficient (only need to solve some fully linear equations at each time step). To achieve such a goal, instead of using traditional discretization approaches like simple implicit [20], stabilized explicit [8, 45, 54, 55, 57–59, 68, 72, 83, 85], convex splitting [67, 88, 89], or other various tricky Taylor expansions [30, 63] to discretize the nonlinear potentials, we adopt the so-called "Invariant Energy Quadratization" (IEQ) method, which is a novel approach and had been successfully applied for various *gradient flow models* in the authors' recent work (cf. [9, 69, 70, 78–82, 86, 87]). The essential idea of the IEQ method is to transform the free energy into a quadratic form (since the nonlinear potential is usually bounded from below) of a set of new variables via a change of variables. The

new, equivalent system still retains the equivalent energy dissipation law in terms of the new variables. Through such a reformulation, all nonlinear terms can be treated semi-explicitly that leads to a well-posed linear system at each time step.

When this IEQ method is applied to the flow coupled model such as the smectic-A model considered in this paper, there are still new challenges due to the nonlinear couplings between the multiple variables, namely, the velocity, the director field as well as the layer, where, in particular, the equation for the velocity is not gradient flow model. To this end, we use the projection method to solve Navier-Stokes equations, and a subtle implicit-explicit treatment to treat the convective and stress terms. Finally we obtain two efficient schemes that are accurate (second order in time), easy-to-implement (linear), and unconditionally energy stable (with a discrete energy dissipation law). Moreover, we rigorously prove that the well-posedness and unconditionally energy stabilities hold for the two proposed schemes, and demonstrate the stability and the accuracy of the proposed schemes through a number of classical benchmark simulation, in particular, the layer motions under shear flow and magnetic force. To the best of the authors' knowledge, the proposed schemes here are the first second order accurate schemes for the flow coupled smectic-A model with unconditional energy stabilities.

The rest of the paper is organized as follows. In Section 2, we present the whole system and show the energy law in the continuous level. In Section 3, we develop the numerical schemes and prove their well-posedness and unconditional stabilities. In Section 4, we present various 2D numerical experiments to demonstrate the stability and the accuracy of the developed numerical schemes in simulating the dynamics under shear flow and the magnetic field. Finally, some concluding remarks are presented in Section 5.

2. Model

We now give a brief introduction for the hydrodynamical smectic-A phase model in [14, 30]. Let $\Omega \subset \mathbb{R}^d$ with $d = 2, 3$ be the bounded domain occupied by the LCs with boundary $\partial\Omega$. The standard Oseen-Frank distortional energy for the bulk free energy takes the following form:

$$(2.1) \qquad E(\boldsymbol{d}) = \int_\Omega \Big(\frac{K_1}{2}(\nabla \cdot \boldsymbol{d})^2 + \frac{K_2}{2}(\boldsymbol{d} \cdot (\nabla \times \boldsymbol{d}))^2 + \frac{K_3}{2}|\boldsymbol{d} \times (\nabla \times \boldsymbol{d})|^2 \Big) d\boldsymbol{x},$$

where the unit vector $\boldsymbol{d}$ represents the average orientation of liquid crystal molecules and K_1, K_2, K_3 are elastic constants for the three canonical distortional modes: splay, twist and bending, respectively. For simplicity, we suppress the anisotropic distortional elastic modes by assuming $K_1 = K_2 = K_3 = K$. Then, the Oseen-Frank energy density reduces to the Dirichlet functional

$$(2.2) \qquad E(\boldsymbol{d}) = K \int_\Omega \frac{1}{2}|\nabla \boldsymbol{d}|^2 d\boldsymbol{x}.$$

For uniaxial smectic LCs, the molecules are aligned in layers with the normal vector $\boldsymbol{n}$. More specific, for smectic-A phase, $\boldsymbol{d}$ is strictly perpendicular to the layers thus $\boldsymbol{d} = \boldsymbol{n}$. Due to the incompressibility of the layers, we have $\nabla \cdot \boldsymbol{n} = 0$, then there exists a layer function $\phi(\boldsymbol{x}, t)$ such that $\nabla\phi = \boldsymbol{n}$. In turn, the Dirichlet functional is reduced to

$$(2.3) \qquad E(\phi) = K \int_\Omega \frac{1}{2}(\Delta\phi)^2 d\boldsymbol{x}, \text{ with } |\nabla\phi| = 1.$$

The norm 1 constraint applied to $|\nabla\phi|$ can bring up some additional numerical challenges in algorithm designs. A common technique to overcome it is to introduce a penalty term of the Ginzburg-Landau type $F(\nabla\phi) = \frac{1}{4\epsilon^2}(|\nabla\phi|^2 - 1)^2$ with $\epsilon \ll 1$ to regularize the distortional energy in the cores of topological defects [30, 41, 45, 87, 89, 90], where ϵ is a penalization parameter that is

proportional to the size of the defect core (or zone). This regularization allows the free energy to be finite at the defect core, extending the classical Ericksen-Leslie model to handle liquid crystal flows where defects are created and annihilated in time and space. Then, the regularized elastic bulk energy density is given by

$$(2.4) \qquad E(\phi) = K \int_\Omega \Big(\frac{1}{2} |\Delta\phi|^2 + \frac{(|\nabla\phi|^2 - 1)^2}{4\epsilon^2} \Big) d\boldsymbol{x}.$$

Assuming $\boldsymbol{u}$ is the fluid velocity field and applying the generalized Fick's law that the mass flux is proportional to the gradient of the chemical potential [3,4,44], we have the following hydrodynamical model for the smectic-A phase LCs system [14,30]:

$$(2.5) \qquad \phi_t + \nabla \cdot (\boldsymbol{u}\phi) = -Mw,$$

$$(2.6) \qquad w = \frac{\delta E}{\delta\phi} = K(\Delta^2\phi - \frac{1}{\epsilon^2}\nabla \cdot (|\nabla\phi|^2 - 1)\nabla\phi)),$$

$$(2.7) \qquad \boldsymbol{u}_t + (\boldsymbol{u} \cdot \nabla)\boldsymbol{u} - \nabla \cdot \sigma(\boldsymbol{u}, \phi) + \nabla p + \phi\nabla w = 0,$$

$$(2.8) \qquad \nabla \cdot \boldsymbol{u} = 0,$$

where p is the pressure, M is the elastic relaxation time, σ is the dissipative (symmetric) stress tensor given in [14] that reads as,

$$(2.9) \qquad \begin{aligned} \sigma(\boldsymbol{u}, \phi) =& \mu_1 \big(\nabla\phi^T D(\boldsymbol{u})\nabla\phi \big) \nabla\phi \otimes \nabla\phi + \mu_4 D(\boldsymbol{u}) \\ & + \mu_5 \big(D(\boldsymbol{u})\nabla\phi \otimes \nabla\phi + \nabla\phi \otimes D(\boldsymbol{u})\nabla\phi \big), \end{aligned}$$

where μ_1, μ_4, μ_5 are nonnegative parameters, and $D(\boldsymbol{u}) = \frac{1}{2}(\nabla\boldsymbol{u} + \nabla\boldsymbol{u}^T)$ is a deformation tensor. We set the non-slip boundary condition for $\boldsymbol{u}$ and the following boundary conditions for ϕ to remove all boundary integral terms,

$$(2.10) \qquad \boldsymbol{u}|_{\partial\Omega} = 0, \quad \partial_{\boldsymbol{m}}(\Delta\phi)|_{\partial\Omega} = 0, \quad \partial_{\boldsymbol{m}}\phi|_{\partial\Omega} = 0,$$

where $\boldsymbol{m}$ is the outward normal on the boundary. It is easy to see that the equation (2.5) is mass-conserved for the layer function ϕ, i.e., $\frac{d}{dt}\int_\Omega \phi dx = 0$.

We can easily derive the PDE energy dissipation law for the above model. Here and after, for any function $f, g \in L^2(\Omega)$, we use $(f, g) = \int_\Omega f(\boldsymbol{x})g(\boldsymbol{x})d\boldsymbol{x}$ to denote the L^2 inner product between functions $f(\boldsymbol{x})$ and $g(\boldsymbol{x})$, and $\|f\|^2 = (f, f)$.

By taking the L^2 inner product of (2.5) with w, of (2.6) with ϕ_t, of (2.7) with $\boldsymbol{u}$, and summing up the obtained equalities, we can obtain

$$(2.11) \qquad \begin{aligned} & \frac{d}{dt} \int_\Omega \Big(\frac{1}{2} |\boldsymbol{u}|^2 + K \big(\frac{1}{2} |\Delta\phi|^2 + \frac{(|\nabla\phi|^2 - 1)^2}{4\epsilon^2} \big) \Big) d\boldsymbol{x} \\ & = - \int_\Omega \Big(\mu_1 (\nabla\phi^T D(\boldsymbol{u})\nabla\phi)^2 + \mu_4 |D(\boldsymbol{u})|^2 + 2\mu_5 |D(\boldsymbol{u})\nabla\phi|^2 + M|w|^2 \Big) d\boldsymbol{x} \le 0, \end{aligned}$$

Even though the above PDE energy law is straightforward, the variable w involves the fourth order derivative of $\Delta^2\phi$, and it is not convenient to use them as test functions in numerical approximations. This makes it difficult to prove the energy dissipation law in the discrete level. To overcome it, we can reformulate the momentum equation (2.7) to an equivalent form which is more applicable for numerical approximations.

Define $\dot{\phi} = \phi_t + \nabla \cdot (\boldsymbol{u}\phi), \psi = -\Delta\phi$, and notice that $w = -\frac{\dot{\phi}}{M}$, then (2.5)-(2.7) can be rewritten as,

$$(2.12) \qquad \frac{\dot{\phi}}{M} = K\Delta\psi + \frac{K}{\epsilon^2}\nabla \cdot (|\nabla\phi|^2 - 1)\nabla\phi)),$$

$$(2.13) \qquad \psi = -\Delta\phi,$$

$$(2.14) \qquad \boldsymbol{u}_t + (\boldsymbol{u} \cdot \nabla)\boldsymbol{u} - \nabla \cdot \sigma(\boldsymbol{u}, \phi) + \nabla p - \frac{1}{M}\phi\nabla\dot{\phi} = 0.$$

$$(2.15) \qquad \nabla \cdot \boldsymbol{u} = 0.$$

with the boundary conditions as

$$(2.16) \qquad \boldsymbol{u}|_{\partial\Omega} = 0, \quad \partial_{\boldsymbol{m}}\psi|_{\partial\Omega} = 0, \quad \partial_{\boldsymbol{m}}\phi|_{\partial\Omega} = 0,$$

This equivalent system (2.12)-(2.15) still admits the similar energy law. We take the time derivative for (2.13) to obtain

$$(2.17) \qquad \psi_t = -\Delta\phi_t,$$

Thus, by taking the L^2 inner product of (2.12) with ϕ_t, of (2.17) with $K\psi$, of (2.14) with $\boldsymbol{u}$, using the incompressible condition (2.15), and summing them up, one can obtain the similar energy law as follows,

$$(2.18) \qquad \begin{aligned} &\frac{d}{dt}\int_\Omega \Big(\frac{1}{2}|\boldsymbol{u}|^2 + \frac{K}{2}|\psi|^2 + \frac{K}{4\epsilon^2}(|\nabla\phi|^2 - 1)^2\Big)d\boldsymbol{x} \\ &= -\int_\Omega \Big(\mu_1(\nabla\phi^T D(\boldsymbol{u})\nabla\phi)^2 + \mu_4|D(\boldsymbol{u})|^2 + 2\mu_5|D(\boldsymbol{u})\nabla\phi|^2 + \frac{1}{M}|\dot{\phi}|^2\Big)d\boldsymbol{x} \leq 0, \end{aligned}$$

Note that the above derivation is suitable in a finite dimensional approximation since the test functions ϕ_t and ψ are both in the same subspaces as ϕ. Hence, it allows us to design numerical schemes which satisfy the energy dissipation law in the discrete level.

Remark 2.1. *In [13], de Genes et. al. presented a total free energy of smectic-A phase LCs that is described by the director field $\boldsymbol{d}$ and a complex order parameter Ψ that represents the average direction of molecular alignment and the layer structure, respectively. The smectic order parameter is written as $\Psi(\boldsymbol{x}) = \rho(\boldsymbol{x})e^{iq\omega(\boldsymbol{x})}$, where $\omega(\boldsymbol{x})$ is the order parameter to describe the layer structure so that $\nabla\omega$ is perpendicular to the layer, and the smectic layer density $\rho(\boldsymbol{x})$ is the mass density of the layers. Thus the total free energy proposed by de Genes et. al. reads as follows,*

$$(2.19) \qquad E(\Psi, \boldsymbol{d}) = \int_\Omega \Big(C|\nabla\Psi - iq\boldsymbol{d}\Psi|^2 + K|\nabla\boldsymbol{d}|^2 + \frac{g}{2}(|\Psi|^2 - \frac{r}{g})^2\Big)d\boldsymbol{x},$$

where the order parameters C, k, g, r are all fixed positive constants. By assuming the density $\rho(x) = r/g$ and $\phi(\boldsymbol{x}) = \frac{\omega(\boldsymbol{x})}{d}$ and rescaling other parameters, one can obtain the normalized energy as (cf. [24]),

$$(2.20) \qquad E(\phi, \boldsymbol{d}) = \int_\Omega \Big(\frac{|\nabla\phi - \boldsymbol{d}|^2}{2\eta^2} + \frac{|\nabla\boldsymbol{d}|^2}{2}\Big)d\boldsymbol{x}.$$

where η is a constant determined by the domain size and other parameters. Therefore, the free energy (2.3) can be viewed the approximation of the de Genes' energy when $\eta \to 0$.

3. Numerical schemes

We now construct time marching schemes for solving the model system (2.12)-(2.15). Our aim is to construct schemes that are not only easy-to-implement, but also unconditionally energy stable.

Here the term easy-to-implement is referred to "linear" and "decoupled" in comparison with its counter parts: "nonlinear" and "coupled". Thus we use the IEQ approach to discretize the double well potential since it is an efficient linear approach, and the projection methods for the Navier-Stokes equation [28, 29, 62] since it can decouple the calculations of the pressure from the velocity field. The key point of IEQ method is to make the nonlinear potential quadratic. More precisely, we define an auxiliary function U as

$$(3.1) \qquad U = |\nabla\phi|^2 - 1,$$

thus the total energy of (4.7) turns to a new form as

$$(3.2) \qquad E(\phi, U) = K \int_\Omega \Big(\frac{1}{2}(\Delta\phi)^2 + \frac{1}{4\epsilon^2}U^2\Big)d\boldsymbol{x}.$$

Then we obtain an equivalent PDE system by taking the time derivative for the new variable U:

$$(3.3) \qquad \frac{\dot{\phi}}{M} = K\Delta\psi + \frac{K}{\epsilon^2}\nabla\cdot(U\nabla\phi)),$$

$$(3.4) \qquad \psi = -\Delta\phi,$$

$$(3.5) \qquad U_t = 2\nabla\phi\cdot\nabla\phi_t,$$

$$(3.6) \qquad \boldsymbol{u}_t + (\boldsymbol{u}\cdot\nabla)\boldsymbol{u} - \nabla\cdot\sigma(\boldsymbol{u}, \phi) + \nabla p - \frac{1}{M}\phi\nabla\dot{\phi} = 0,$$

$$(3.7) \qquad \nabla\cdot\boldsymbol{u} = 0.$$

The boundary conditions for the new system are still (2.10) since the equation (3.5) for the new variable U is simply an ODE with time. The initial conditions read as

$$(3.8) \qquad \boldsymbol{u}|_{(t=0)} = \boldsymbol{u}_0,\ \phi|_{(t=0)} = \phi_0,\ U|_{(t=0)} = |\nabla\phi_0|^2 - 1.$$

It is clear that the new equivalent system (3.3)-(3.7) still retains the similar energy law. By taking the L^2 inner product of (3.3) with ϕ_t, taking the time derivative of (3.4) and the L^2 inner product with $K\psi$, of (3.5) with $\frac{K}{2\epsilon^2}U$, of (3.6) with $\boldsymbol{u}$, using the incompressible condition (3.7), and summing the obtained equalities up, one can obtain the similar energy law as follows,

$$(3.9)\frac{d}{dt}E(\boldsymbol{u}, \psi, U) = -\int_\Omega \Big(\mu_1(\nabla\phi^T D(\boldsymbol{u})\nabla\phi)^2 + \mu_4|D(\boldsymbol{u})|^2 + 2\mu_5|D(\boldsymbol{u})\nabla\phi|^2 + \frac{1}{M}|\dot{\phi}|^2\Big)d\boldsymbol{x} \leq 0.$$

where

$$(3.10) \qquad E(\boldsymbol{u}, \psi, U) = \int_\Omega \Big(\frac{1}{2}|\boldsymbol{u}|^2 + \frac{K}{2}|\psi|^2 + \frac{K}{4\epsilon^2}U^2\Big)d\boldsymbol{x}$$

Remark 3.1. *We emphasize that the new transformed system (3.3)-(3.7) is exactly equivalent to the original system (2.12)-(2.15), since (2.12) can be easily obtained by integrating (3.5) with respect to the time. For the time-continuous case, the potentials in the new free energy (3.10) are the same as the Lyapunov functional in the original free energy of (2.11). We will develop unconditionally energy stable numerical schemes for time stepping of the transformed system (3.3)-(3.7), and the proposed schemes should formally follow the new energy dissipation law (3.9) in the discrete sense, instead of the energy law for the originated system (2.11).*

3.1. Crank-Nicolson Scheme.
Let $\delta t > 0$ denote the time step size and set $t^n = n\,\delta t$ for $0 \leq n \leq N$ with the ending time $T = N\,\delta t$. We first develop a second order scheme that is based on the Crank-Nicolson, that reads as follows.

Scheme 1. *Having computed $\phi^n, U^n, \boldsymbol{u}^n, p^n$, we update $\phi^{n+1}, U^{n+1}, \boldsymbol{u}^{n+1}, p^{n+1}$ as follows (we compute $\phi^1, U^1, \boldsymbol{u}^1, p^1$ by assuming $\phi^{-1} = \phi^0, \psi^{-1} = \psi^0 = -\Delta\phi^0, U^{-1} = U^0, \boldsymbol{u}^{-1} = \boldsymbol{u}^0, p^{-1} = p^0$ for the initial step):*

Step 1:

$$(3.11) \qquad \frac{1}{M}\dot{\phi}^{n+1} = K\Delta\psi^{n+\frac{1}{2}} + \frac{K}{\epsilon^2}\nabla\cdot(U^{n+\frac{1}{2}}\nabla\phi^{\star,n+\frac{1}{2}}),$$

$$(3.12) \qquad \psi^{n+1} = -\Delta\phi^{n+1},$$

$$(3.13) \qquad U^{n+1} - U^n = 2\nabla\phi^{\star,n+\frac{1}{2}}\cdot(\nabla\phi^{n+1} - \nabla\phi^n),$$

$$(3.14) \qquad \frac{\widetilde{\boldsymbol{u}}^{n+1} - \boldsymbol{u}^n}{\delta t} + B(\boldsymbol{u}^{\star,n+\frac{1}{2}}, \widetilde{\boldsymbol{u}}^{n+\frac{1}{2}}) - \nabla\cdot\sigma(\widetilde{\boldsymbol{u}}^{n+\frac{1}{2}}, \phi^{\star,n+\frac{1}{2}}) + \nabla p^n - \frac{1}{M}\phi^{\star,n+\frac{1}{2}}\nabla\dot{\phi}^{n+1} = 0,$$

with the boundary conditions

$$(3.15) \qquad \widetilde{\boldsymbol{u}}^{n+1}|_{\partial\Omega} = 0, \partial_{\boldsymbol{m}}\phi^{n+1} = \partial_{\boldsymbol{m}}\psi^{n+1}|_{\partial\Omega} = 0,$$

where

$$(3.16) \qquad \begin{cases} B(\boldsymbol{u}, \boldsymbol{v}) = (\boldsymbol{u}\cdot\nabla)\boldsymbol{v} + \dfrac{1}{2}(\nabla\cdot\boldsymbol{u})\boldsymbol{v}, \\[2mm] \phi^{\star,n+\frac{1}{2}} = \dfrac{3}{2}\phi^n - \dfrac{1}{2}\phi^{n-1}, \ \boldsymbol{u}^{\star,n+\frac{1}{2}} = \dfrac{3}{2}\boldsymbol{u}^n - \dfrac{1}{2}\boldsymbol{u}^{n-1}, \\[2mm] \psi^{n+\frac{1}{2}} = \dfrac{\psi^{n+1} + \psi^n}{2}, \ \widetilde{\boldsymbol{u}}^{n+\frac{1}{2}} = \dfrac{\widetilde{\boldsymbol{u}}^{n+1} + \boldsymbol{u}^n}{2}, \ U^{n+\frac{1}{2}} = \dfrac{U^{n+1} + U^n}{2}, \\[2mm] \dot{\phi}^{n+1} = \dfrac{\phi^{n+1} - \phi^n}{\delta t} + \nabla\cdot(\widetilde{\boldsymbol{u}}^{n+\frac{1}{2}}\phi^{\star,n+\frac{1}{2}}). \end{cases}$$

Step 2:

$$(3.17) \qquad \frac{\boldsymbol{u}^{n+1} - \widetilde{\boldsymbol{u}}^{n+1}}{\delta t} + \frac{1}{2}\nabla(p^{n+1} - p^n) = 0,$$

$$(3.18) \qquad \nabla\cdot\boldsymbol{u}^{n+1} = 0, \ \boldsymbol{u}^{n+1}\cdot\boldsymbol{m}|_{\partial\Omega} = 0.$$

Remark 3.2. *Here, for solving the Navier-Stokes equation, we use a second order pressure correction scheme [64] to decouple the computations of pressure from that of the velocity. This projection methods are analyzed in [53] where it is shown (discrete time, continuous space) that the schemes are second order accurate for velocity in $\ell^2(0, T; L^2(\Omega))$ but only first order accurate for pressure in $\ell^\infty(0, T; L^2(\Omega))$. The loss of accuracy for pressure is due to the artificial boundary condition (3.17) imposed on pressure [15, 28]. One can use the rotational projection type schemes to improve the order of pressure to $3/2$. However, how to prove the energy stability for the corresponding schemes are open questions. We also remark that the Crank-Nicolson scheme with linear extrapolation is a popular time discretization for the Navier-Stokes equation. We refer to [28, 36] and references therein for analysis on this type of discretization.*

Schemes (3.11)-(3.14) is totally linear scheme since we handle the convective and stress term by compositions of implicit (Crank-Nicolson) and explicit (second order extrapolation) discretization. Apparently, the new variable U brings up some extra computational cost. But actually, we do not need to calculate U^{n+1} explicitly in every step. By rewriting (3.13), we obtain

$$(3.19) \qquad U^{n+\frac{1}{2}} = S^n + \nabla\phi^{\star,n+\frac{1}{2}}\cdot\nabla\phi^{n+1},$$

where $S^n = U^n - \nabla\phi^{\star,n+\frac{1}{2}} \cdot \nabla\phi^n$. Then (3.11) and (3.14) can be written as the following system with unknowns $(\phi, \boldsymbol{u})$, where ϕ^{n+1} and $\widetilde{\boldsymbol{u}}^{n+1}$ are its solutions,

$$(3.20) \qquad \phi + \frac{\delta t}{2}\nabla \cdot (\boldsymbol{u}\phi^{\star,n+\frac{1}{2}}) + \frac{KM\delta t}{2}\Delta^2\phi - \frac{KM\delta t}{\epsilon^2}\nabla \cdot (\nabla\phi^{\star,n+\frac{1}{2}} \cdot \nabla\phi)\nabla\phi^{\star,n+\frac{1}{2}} = f_1,$$

$$(3.21) \qquad \frac{\delta t M}{2}\boldsymbol{u} + \frac{\delta t^2 M}{4}B(\boldsymbol{u}^{\star,n+\frac{1}{2}},\boldsymbol{u}) - \frac{M\delta t^2}{4}\nabla \cdot \sigma(\boldsymbol{u},\phi^{\star,n+\frac{1}{2}})$$
$$- \frac{\delta t}{2}\nabla\big(\phi + \frac{\delta t}{2}\nabla \cdot (\boldsymbol{u}\phi^{\star,n+\frac{1}{2}})\big)\phi^{\star,n+\frac{1}{2}} = f_2,$$

where f_1 and f_2 are given from previous time steps that read as

$$(3.22) \quad \begin{cases} f_1 = \phi^n - \dfrac{\delta t}{2}\nabla \cdot (\boldsymbol{u}^n\phi^{\star,n+\frac{1}{2}}) + \dfrac{KM\delta t}{2}\psi^n + \dfrac{KM\delta t}{\epsilon^2}\nabla \cdot (S^n\nabla\phi^{\star,n+\frac{1}{2}}), \\[2mm] f_2 = \dfrac{M\delta t}{2}\boldsymbol{u}^n - \dfrac{M\delta t^2}{4}B(\boldsymbol{u}^{\star,n+\frac{1}{2}},\boldsymbol{u}^n) + \dfrac{\delta t^2 M}{4}\nabla \cdot \sigma(\boldsymbol{u}^n,\nabla\phi^{\star,n+\frac{1}{2}}) - \dfrac{M\delta t^2}{2}\nabla p^n \\[2mm] \qquad - \dfrac{\delta t}{2}\phi^{\star,n+\frac{1}{2}}\nabla\big(\phi^n - \dfrac{\delta t}{2}\nabla \cdot (\boldsymbol{u}^n\phi^{\star,n+\frac{1}{2}})\big). \end{cases}$$

We first show the well-posedness of the above linear system (3.20)-(3.21) as follows.

Theorem 3.1. *The linear system (3.20)-(3.21) (or (3.11)-(3.14)) admits a unique solution in $(\phi, \boldsymbol{u}) \in (H^2, H^1)(\Omega)$.*

Proof. By taking the L^2 inner product of (3.11) with 1, we obtain

$$(3.23) \qquad \int_\Omega \phi^{n+1}d\boldsymbol{x} = \int_\Omega \phi^n d\boldsymbol{x} = \cdots = \int_\Omega \phi^0 d\boldsymbol{x}.$$

Let $v_\phi = \frac{1}{|\Omega|}\int_\Omega \phi^0 d\boldsymbol{x}$, and we define $\widehat{\phi} = \phi - v_\phi$. Then $\int_\Omega \widehat{\phi}d\boldsymbol{x} = 0$ and $(\widehat{\phi}, \boldsymbol{u})$ is the solution of the following linear system with unknowns denoted by $(\phi, \boldsymbol{u})$,

$$(3.24) \quad \phi + \frac{\delta t}{2}\nabla \cdot (\boldsymbol{u}\phi^{\star,n+\frac{1}{2}}) + \frac{KM\delta t}{2}\Delta^2\phi - \frac{KM\delta t}{\epsilon^2}\nabla \cdot (\nabla\phi^{\star,n+\frac{1}{2}} \cdot \nabla\phi)\nabla\phi^{\star,n+\frac{1}{2}} = f_1 - v_\phi,$$

$$(3.25) \quad \frac{\delta t M}{2}\boldsymbol{u} + \frac{\delta t^2 M}{4}B(\boldsymbol{u}^{\star,n+\frac{1}{2}},\boldsymbol{u}) - \frac{M\delta t^2}{4}\nabla \cdot \sigma(\boldsymbol{u},\phi^{\star,n+\frac{1}{2}})$$
$$- \frac{\delta t}{2}\nabla\big(\phi + \frac{\delta t}{2}\nabla \cdot (\boldsymbol{u}\phi^{\star,n+\frac{1}{2}})\big)\phi^{\star,n+\frac{1}{2}} = f_2.$$

We denote the above linear system (3.24)-(3.25) as

$$(3.26) \qquad\qquad\qquad \mathbb{A}\boldsymbol{X} = \mathbb{B},$$

with $\boldsymbol{X} = (\phi, \boldsymbol{u})^T$ and $\mathbb{B} = (f_1 - v_\phi, f_2)^T$.

For any $\boldsymbol{X}_1 = (\phi_1, \boldsymbol{u}_1)^T$ and $\boldsymbol{X}_2 = (\phi_2, \boldsymbol{u}_2)^T$ with $\int_\Omega \phi_1 d\boldsymbol{x} = \int_\Omega \phi_2 d\boldsymbol{x} = 0$ with the boundary conditions (3.15), we have

$$(3.27) \qquad \boldsymbol{X}_1^T\mathbb{A}\boldsymbol{X}_2 \le C_1(\|\phi_1\|_{H^2} + \|\boldsymbol{u}_1\|_{H^1})(\|\phi_2\|_{H^2} + \|\boldsymbol{u}_2\|_{H^1}),$$

where $C_1 = C(\delta t, M, \epsilon^2, K, \boldsymbol{u}^{\star,n+\frac{1}{2}}, \phi^{\star,n+\frac{1}{2}}, \phi^n, \mu_1, \mu_4, \mu_5)$.

For any $\boldsymbol{X} = (\phi, \boldsymbol{u})^T$ with $\int_\Omega \phi d\boldsymbol{x} = 0$, we derive

$$
\begin{aligned}
\boldsymbol{X}^T \mathbb{A} \boldsymbol{X} =& \|\phi + \frac{\delta t}{2} \boldsymbol{u} \nabla \phi^{\star,n+\frac{1}{2}}\|^2 + \frac{KM\delta t}{2}\|\Delta\phi\|^2 + \frac{KM\delta t}{\epsilon^2}\|\nabla\phi^{\star,n+\frac{1}{2}}\nabla\phi\|^2 + \frac{\delta t M}{2}\|\boldsymbol{u}\|^2 \\
(3.28) \qquad & + \frac{M\delta t^2}{4}\Big(\mu_1\|(\nabla\phi^{\star,n+\frac{1}{2}})^T D(\boldsymbol{u})\nabla\phi^{\star,n+\frac{1}{2}}\|^2 + \mu_4\|D(\boldsymbol{u})\|^2 + 2\mu_5\|D(\boldsymbol{u})\nabla\phi^{\star,n+\frac{1}{2}}\|^2\Big) \\
& \geq C_2(\|\phi\|_{H^2}^2 + \|\boldsymbol{u}\|_{H^1}^2),
\end{aligned}
$$

where $C_2 = C(\delta t, M, \epsilon^2, K, \boldsymbol{u}^{\star,n+\frac{1}{2}}, \phi^{\star,n+\frac{1}{2}}, \phi^n, \mu_4)$. Then from the Lax-Milgram theorem, we conclude the linear system (3.26) admits a unique solution $(\phi, \boldsymbol{u}) \in (H^2, H^1)(\Omega)$.

$\square$

The energy stability of the scheme (3.11)-(3.18) is presented as follows.

Theorem 3.2. *The scheme* (3.11)-(3.18) *is unconditionally energy stable satisfying the following discrete energy dissipation law,*

$$
\begin{aligned}
(3.29) \quad E_{tot-cn2}^{n+1} = E_{tot-cn2}^n &- \frac{\delta t}{M}\|\dot{\phi}^{n+1}\|^2 - \delta t\Big(\mu_1\|(\nabla\phi^{\star,n+\frac{1}{2}})^T D(\widetilde{\boldsymbol{u}}^{n+\frac{1}{2}})\nabla\phi^{\star,n+\frac{1}{2}}\|^2 \\
&+ \mu_4\|D(\widetilde{\boldsymbol{u}}^{n+\frac{1}{2}})\|^2 + \mu_5\|D(\widetilde{\boldsymbol{u}}^{n+\frac{1}{2}})\nabla\phi^{\star,n+\frac{1}{2}}\|^2\Big),
\end{aligned}
$$

where

$$
(3.30) \qquad E_{tot-cn2}^n = \frac{1}{2}\|\boldsymbol{u}^n\|^2 + \frac{K}{2}\|\psi^n\|^2 + \frac{K}{4\epsilon^2}\|U^n\|^2 + \frac{\delta t^2}{8}\|\nabla p^n\|^2.
$$

Proof. By taking the L^2 inner product of (3.11) with $\frac{\phi^{n+1}-\phi^n}{\delta t}$ and using integration by parts, we obtain

$$
\begin{aligned}
(3.31) \quad & \frac{1}{M}\|\dot{\phi}^{n+1}\|^2 + \frac{1}{M}(\nabla\dot{\phi}^{n+1}, \widetilde{\boldsymbol{u}}^{n+\frac{1}{2}}\phi^{\star,n+\frac{1}{2}}) \\
& = \frac{K}{\delta t}(\Delta\psi^{n+\frac{1}{2}}, \phi^{n+1} - \phi^n) - \frac{K}{\delta t\epsilon^2}\Big(U^{n+\frac{1}{2}}\nabla\phi^{\star,n+\frac{1}{2}}, \nabla(\phi^{n+1} - \phi^n)\Big).
\end{aligned}
$$

We take the subtraction between $n+1$ step and n step for (3.12) to obtain

$$
(3.32) \qquad \psi^{n+1} - \psi^n = -\Delta(\phi^{n+1} - \phi^n).
$$

By taking the L^2 inner product of (3.32) with $\frac{K}{\delta t}\psi^{n+\frac{1}{2}}$ and using integration by parts, we obtain

$$
\begin{aligned}
(3.33) \quad \frac{K}{2\delta t}(\|\psi^{n+1}\|^2 - \|\psi^n\|^2) &= -\frac{K}{\delta t}(\Delta(\phi^{n+1} - \phi^n), \psi^{n+\frac{1}{2}}) \\
&= -\frac{K}{\delta t}(\phi^{n+1} - \phi^n, \Delta\psi^{n+\frac{1}{2}}).
\end{aligned}
$$

By taking the L^2 inner product of (3.13) with $\frac{K}{2\epsilon^2\delta t}U^{n+\frac{1}{2}}$, we obtain

$$
(3.34) \qquad \frac{K}{4\epsilon^2\delta t}(\|U^{n+1}\|^2 - \|U^n\|^2) = \frac{K}{\epsilon^2\delta t}\Big(\nabla\phi^{\star,n+\frac{1}{2}}(\nabla\phi^{n+1} - \nabla\phi^n), U^{n+\frac{1}{2}}\Big).
$$

By taking the L^2 inner product of (3.14) with $\widetilde{\boldsymbol{u}}^{n+\frac{1}{2}}$, we obtain

$$
\begin{aligned}
(3.35) \quad \frac{1}{2\delta t}(\|\widetilde{\boldsymbol{u}}^{n+1}\|^2 - \|\boldsymbol{u}^n\|^2) &+ \Big(\sigma(\widetilde{\boldsymbol{u}}^{n+\frac{1}{2}}, \nabla\phi^{\star,n+\frac{1}{2}}), \nabla\widetilde{\boldsymbol{u}}^{n+\frac{1}{2}}\Big) + (\nabla p^n, \widetilde{\boldsymbol{u}}^{n+\frac{1}{2}}) \\
&- \frac{1}{M}\Big(\phi^{\star,n+\frac{1}{2}}\nabla\dot{\phi}^{n+1}, \widetilde{\boldsymbol{u}}^{n+\frac{1}{2}}\Big) = 0.
\end{aligned}
$$

By taking the L^2 inner product of (3.17) with $\boldsymbol{u}^{n+1}$ and performing integration by parts, we have

$$(3.36) \qquad \frac{1}{2\delta t}(\|\boldsymbol{u}^{n+1}\|^2 - \|\widetilde{\boldsymbol{u}}^{n+1}\|^2 + \|\boldsymbol{u}^{n+1} - \widetilde{\boldsymbol{u}}^{n+1}\|^2) = 0,$$

where we use explicitly the divergence-free condition for $\boldsymbol{u}^{n+1}$ as

$$(3.37) \qquad (\nabla(p^{n+1} - p^n), \boldsymbol{u}^{n+1}) = -((p^{n+1} - p^n), \nabla \cdot \boldsymbol{u}^{n+1}) = 0.$$

We rewrite the projection step (3.17) as

$$(3.38) \qquad \frac{1}{\delta t}(\boldsymbol{u}^{n+1} + \boldsymbol{u}^n - 2\widetilde{\boldsymbol{u}}^{n+\frac{1}{2}}) + \frac{1}{2}\nabla(p^{n+1} - p^n) = 0.$$

By taking the inner product of the above equation with $\frac{\delta t}{2}\nabla p^n$, one arrives at

$$(3.39) \qquad \frac{\delta t}{8}\left(\|\nabla p^{n+1}\|^2 - \|\nabla p^n\|^2 - \|\nabla(p^{n+1} - p^n)\|^2\right) = \left(\nabla p^n, \widetilde{\boldsymbol{u}}^{n+\frac{1}{2}}\right).$$

On the other hand, it follows directly from (3.17) that

$$(3.40) \qquad \frac{\delta t}{8}\|\nabla(p^{n+1} - p^n)\|^2 = \frac{1}{2\delta t}\|\boldsymbol{u}^{n+1} - \widetilde{\boldsymbol{u}}^{n+1}\|^2.$$

Finally, by combining (3.31), (3.33), (3.34)-(3.36), (3.39) and (3.40), we obtain

$$
\begin{aligned}
(3.41) \qquad & \frac{1}{M}\|\dot{\phi}^{n+1}\|^2 + \frac{K}{2\delta t}(\|\psi^{n+1}\|^2 - \|\psi^n\|^2) + \frac{K}{4\epsilon^2 \delta t}(\|U^{n+1}\|^2 - \|U^n\|^2) \\
& \quad + \frac{\delta t}{8}(\|\nabla p^{n+1}\|^2 - \|\nabla p^n\|^2) + \frac{1}{2\delta t}(\|\boldsymbol{u}^{n+1}\|^2 - \|\boldsymbol{u}^n\|^2) \\
& \quad + \left(\sigma(\widetilde{\boldsymbol{u}}^{n+\frac{1}{2}}, \nabla\phi^{\star,n+\frac{1}{2}}), \nabla\widetilde{\boldsymbol{u}}^{n+\frac{1}{2}}\right) = 0.
\end{aligned}
$$

$\square$

Remark 3.3. *One can formally verify that the energy law (3.29) is a second order approximation of the continuous energy law (3.9) at time level $t^{n+\frac{1}{2}}$.*

Remark 3.4. *We notice that the idea of the IEQ approach is very simple but quite different from the traditional time marching schemes. For example, it does not require the convexity as the convex splitting approach (cf. [18]) or the boundness for the second order derivative as the linear stabilization approach (cf. [55, 56, 65]). Through a simple substitution of new variables, the complicated nonlinear potentials are transformed into quadratic forms. We summarize the great advantages of this quadratic transformations as follows: (i) this quadratization method works well for various complex nonlinear terms as long as the corresponding nonlinear potentials are bounded from below; (ii) the complicated nonlinear potential is transferred to a quadratic polynomial form which is much easier to handle; (iii) the derivative of the quadratic polynomial is linear, which provides the fundamental support for linearization method; (iv) the quadratic formulation in terms of new variables can automatically maintain this property of positivity (or bounded from below) of the nonlinear potentials.*

Remark 3.5. *We remark that when the nonlinear potential takes the fourth order polynomial type, e.g. $F(\psi) = (\psi^2 - 1)^2$ where $\psi = \phi$ for Cahn-Hilliard equation and $\psi = |\nabla\phi|$ for the smectic model in this paper or the MBE model [81], this IEQ method is exactly the same as the Lagrange multiplier method in [31, 63]. But the Lagrange multiplier method will only work the fourth order polynomial type potential since its derivative ψ^3 can be decomposed into $\lambda(\psi)\psi$ with $\lambda(\psi) = |\psi|^2$ which can be viewed as a Lagrange multiplier term. However, for other type potentials, the Lagrange multiplier method is not applicable. About the application of the IEQ approach to handle other*

type of nonlinear potentials, e.g., the logarithmic Flory-Huggins potential, or anisotropic gradient entropy, etc., we refer to the authors' other work in [69, 78, 79, 81, 86, 87].

3.2. **Adam-bashforth Scheme.** We further develop another second order version scheme based on the backward differentiation formula with the Adam-Bashforth explicit interpolation (BDF2), that reads as follows.

Scheme 2. *Having computed the numerical solutions of $(\phi, U, \boldsymbol{u}, p)$ at t^n and t^{n-1}, we update $\phi^{n+1}, U^{n+1}, \boldsymbol{u}^{n+1}, p^{n+1}$ as follows:*

Step 1:

$$(3.42) \qquad \frac{1}{M}\dot{\phi}^{n+1} = K\Delta\psi^{n+1} + \frac{K}{\epsilon^2}\nabla\cdot(U^{n+1}\nabla\phi^{*,n+1})$$

$$(3.43) \qquad \psi^{n+1} = -\Delta\phi^{n+1},$$

$$(3.44) \qquad 3U^{n+1} - 4U^n + U^{n-1} = 2\nabla\phi^{*,n+1}\cdot(3\nabla\phi^{n+1} - 4\nabla\phi^n + \nabla\phi^{n-1})$$

$$(3.45) \qquad \frac{3\widetilde{\boldsymbol{u}}^{n+1} - 4\boldsymbol{u}^n + \boldsymbol{u}^{n-1}}{2\delta t} + B(\boldsymbol{u}^{*,n+1}, \widetilde{\boldsymbol{u}}^{n+1}) - \nabla\cdot\sigma(\widetilde{\boldsymbol{u}}^{n+1}, \phi^{*,n+1}) + \nabla p^n$$
$$-\frac{1}{M}\phi^{*,n+1}\nabla\dot{\phi}^{n+1} = 0,$$

with the boundary conditions

$$(3.46) \qquad \widetilde{\boldsymbol{u}}^{n+1}|_{\partial\Omega} = 0, \ \partial_{\boldsymbol{m}}\phi^{n+1}|_{\partial\Omega} = \partial_{\boldsymbol{m}}\psi^{n+1}|_{\partial\Omega} = 0,$$

where

$$(3.47) \qquad \begin{cases} \boldsymbol{u}^{*,n+1} = 2\boldsymbol{u}^n - \boldsymbol{u}^{n-1}, \phi^{*,n+1} = 2\phi^n - \phi^{n-1}, \\ \dot{\phi}^{n+1} = \dfrac{3\phi^{n+1} - 4\phi^n + \phi^{n-1}}{2\delta t} + \nabla\cdot(\widetilde{\boldsymbol{u}}^{n+1}\phi^{*,n+1}). \end{cases}$$

Step 2:

$$(3.48) \qquad 3\frac{\boldsymbol{u}^{n+1} - \widetilde{\boldsymbol{u}}^{n+1}}{2\delta t} + \nabla(p^{n+1} - p^n) = 0,$$

$$(3.49) \qquad \nabla\cdot\boldsymbol{u}^{n+1} = 0, \ \boldsymbol{u}^{n+1}\cdot\boldsymbol{m}|_{\partial\Omega} = 0.$$

Similar to the Crank-Nicolson scheme, one can rewrite the equations (3.5) as follows:

$$(3.50) \qquad U^{n+1} = Z^n + 2\nabla\phi^{*,n+1}\cdot\nabla\phi^{n+1},$$

where $Z^n = \frac{4U^n - U^{n-1}}{3} - 2\nabla\phi^{*,n+1}\cdot\frac{4\nabla\phi^n - \nabla\phi^{n-1}}{3}$. Then ϕ^{n+1} and $\widetilde{\boldsymbol{u}}^{n+1}$ are the solutions for the following system with unknowns $(\phi, \boldsymbol{u})$,

$$(3.51) \qquad \phi + \frac{2\delta t}{3}\nabla\cdot(\boldsymbol{u}\phi^{*,n+1}) + \frac{2KM\delta t}{3}\Delta^2\phi - \frac{4KM\delta t}{3\epsilon^2}\nabla\cdot((\nabla\phi^{*,n+1}\cdot\nabla\phi)\nabla\phi^{*,n+1}) = g_1,$$

$$(3.52) \qquad \frac{2\delta t M}{3}\boldsymbol{u} + \frac{4\delta t^2 M}{9}\boldsymbol{u}^{*,n+1}\cdot\nabla\boldsymbol{u} - \frac{4M\delta t^2}{9}\nabla\cdot\sigma(\boldsymbol{u}, \phi^{*,n+1})$$
$$-\frac{2\delta t}{3}\phi^{*,n+1}\nabla\big(\phi + \frac{2\delta t}{3}\nabla\cdot(\boldsymbol{u}\phi^{*,n+1})\big) = g_2,$$

where

$$(3.53) \qquad \begin{cases} g_1 = \dfrac{4\phi^n - \phi^{n-1}}{3} + \dfrac{2KM\delta t}{3\epsilon^2}\nabla\cdot(Z^n\nabla\phi^{*,n+1}), \\ g_2 = \dfrac{2M\delta t}{9}(4\boldsymbol{u}^n - \boldsymbol{u}^{n-1}) - \dfrac{4M\delta t^2}{9}\nabla p^n - \dfrac{2\delta t}{9}\phi^{*,n+1}\nabla(4\phi^n - \phi^{n-1}). \end{cases}$$

Theorem 3.3. *The linear system* (3.42)-(3.45) *(or* (3.51)-(3.52)*) admits a unique solution in* $(\phi, \boldsymbol{u}) \in (H^2, H^1)(\Omega)$.

Proof. The proof of well-posedness is similar to Theorem 3.1, thus we omit the details here. $\quad\square$

Theorem 3.4. *The scheme* (3.42)-(3.49) *is unconditionally energy stable satisfying the following discrete energy dissipation law,*

$$
(3.54) \quad E_{tot-bdf2}^{n+1} \leq E_{tot-bdf2}^n - \frac{\delta t}{M} \|\dot{\phi}^{n+1}\|^2 - \delta t \Big(\mu_1 \|(\nabla \phi^{*,n+1})^T D(\widetilde{\boldsymbol{u}}^{n+1}) \nabla \phi^{*,n+1}\|^2
$$
$$
+ \mu_4 \|D(\widetilde{\boldsymbol{u}}^{n+1})\|^2 + \mu_5 \|D(\widetilde{\boldsymbol{u}}^{n+1}) \nabla \phi^{*,n+1}\|^2 \Big),
$$

where

$$
(3.55) \quad E_{tot-bdf2}^{n+1} = \frac{1}{2} \Big(\frac{\|\boldsymbol{u}^{n+1}\|^2}{2} + \frac{\|2\boldsymbol{u}^{n+1} - \boldsymbol{u}^n\|^2}{2} \Big) + \frac{K}{2} \Big(\frac{\|\psi^{n+1}\|^2}{2} + \frac{\|2\psi^{n+1} - \psi^n\|^2}{2} \Big)
$$
$$
+ \frac{K}{4\epsilon^2} \Big(\frac{\|U^{n+1}\|^2}{2} + \frac{\|2U^{n+1} - U^n\|^2}{2} \Big) + \frac{\delta t^2}{3} \|\nabla p^{n+1}\|^2.
$$

Proof. By taking the L^2 inner product of (3.42) with $\frac{3\phi^{n+1} - 4\phi^n + \phi^{n-1}}{2\delta t}$, we obtain

$$
(3.56) \quad \frac{1}{M} \|\dot{\phi}^{n+1}\|^2 + \frac{1}{M} \Big(\nabla \dot{\phi}^{n+1}, \widetilde{\boldsymbol{u}}^{n+1} \phi^{*,n+1} \Big) = \frac{K}{2\delta t} (\Delta \psi^{n+1}, 3\phi^{n+1} - 4\phi^n + \phi^{n-1})
$$
$$
- \frac{K}{2\delta t \epsilon^2} \Big(U^{n+1} \nabla \phi^{*,n+1}, \nabla (3\phi^{n+1} - 4\phi^n + \phi^{n-1}) \Big).
$$

We take the subtraction of (3.43) with n and $n-1$ step to obtain

$$
(3.57) \quad 3\psi^{n+1} - 4\psi^n + \psi^{n-1} = -\Delta(3\phi^{n+1} - 4\phi^n + \phi^{n-1})
$$

By taking the L^2 inner product of (3.57) with $\frac{K}{2\delta t} \psi^{n+1}$, using the integration by parts and the following identity

$$
(3.58) \quad 2(3a - 4b + c, a) = |a|^2 - |b|^2 + |2a - b|^2 - |2b - c|^2 + |a - 2b + c|^2,
$$

we obtain

$$
(3.59) \quad \frac{K}{4\delta t} (\|\psi^{n+1}\|^2 - \|\psi^n\|^2 + \|2\psi^{n+1} - \psi^n\|^2 - \|2\psi^n - \psi^{n-1}\|^2 + \|\psi^{n+1} + 2\psi^n - \psi^{n-1}\|^2)
$$
$$
= -\frac{K}{2\delta t}(3\phi^{n+1} - 4\phi^n + \phi^{n-1}, \Delta \psi^{n+1})
$$

By taking the L^2 inner product of (3.44) with $\frac{K}{4\delta t \epsilon^2} U^{n+1}$ and applying (3.58), we obtain

$$
(3.60) \quad \frac{K}{8\epsilon^2 \delta t} \Big(\|U^{n+1}\|^2 - \|U^n\|^2 + \|2U^{n+1} - U^n\|^2 - \|2U^n - U^{n-1}\|^2 + \|U^{n+1} - 2U^n + U^{n-1}\|^2 \Big)
$$
$$
= \frac{K}{2\delta t \epsilon^2} (\nabla \phi^{*,n+1}(3\nabla \phi^{n+1} - 4\nabla \phi^n + \nabla \phi^{n-1}), U^{n+1}).
$$

By taking the L^2 inner product of (3.14) with $\widetilde{\boldsymbol{u}}^{n+1}$, we obtain

$$
(3.61) \quad (\frac{3\widetilde{\boldsymbol{u}}^{n+1} - 4\boldsymbol{u}^n + \boldsymbol{u}^{n-1}}{2\delta t}, \widetilde{\boldsymbol{u}}^{n+1}) + \Big(\sigma(\widetilde{\boldsymbol{u}}^{n+1}, \nabla \phi^{*,n+1}), \nabla \widetilde{\boldsymbol{u}}^{n+1} \Big) + (\nabla p^n, \widetilde{\boldsymbol{u}}^{n+1})
$$
$$
- \frac{1}{M} \Big(\phi^{*,n+1} \nabla \dot{\phi}^{n+1}, \widetilde{\boldsymbol{u}}^{n+1} \Big) = 0.
$$

From (3.48), for any function $\boldsymbol{v}$ with $\nabla \cdot \boldsymbol{v} = 0$, we can derive

$$
(3.62) \quad (\boldsymbol{u}^{n+1}, \boldsymbol{v}) = (\widetilde{\boldsymbol{u}}^{n+1}, \boldsymbol{v}).
$$

Then for the first term in (3.61), we have

$$\frac{1}{2\delta t}(3\widetilde{\boldsymbol{u}}^{n+1} - 4\boldsymbol{u}^n + \boldsymbol{u}^{n-1}, \widetilde{\boldsymbol{u}}^{n+1})$$

(3.63)

$$= \frac{1}{2\delta t}(3\widetilde{\boldsymbol{u}}^{n+1} - 3\boldsymbol{u}^{n+1}, \widetilde{\boldsymbol{u}}^{n+1}) + \frac{1}{2\delta t}(3\boldsymbol{u}^{n+1} - 4\boldsymbol{u}^n + \boldsymbol{u}^{n+1}, \widetilde{\boldsymbol{u}}^{n+1})$$

$$= \frac{1}{2\delta t}(3\widetilde{\boldsymbol{u}}^{n+1} - 3\boldsymbol{u}^{n+1}, \widetilde{\boldsymbol{u}}^{n+1}) + \frac{1}{2\delta t}(3\boldsymbol{u}^{n+1} - 4\boldsymbol{u}^n + \boldsymbol{u}^{n+1}, \boldsymbol{u}^{n+1})$$

$$= \frac{1}{2\delta t}(3\widetilde{\boldsymbol{u}}^{n+1} - 3\boldsymbol{u}^{n+1}, \widetilde{\boldsymbol{u}}^{n+1} + \boldsymbol{u}^{n+1}) + \frac{1}{2\delta t}(3\boldsymbol{u}^{n+1} - 4\boldsymbol{u}^n + \boldsymbol{u}^{n-1}, \boldsymbol{u}^{n+1})$$

$$= \frac{3}{2\delta t}(\|\widetilde{\boldsymbol{u}}^{n+1}\|^2 - \|\boldsymbol{u}^{n+1}\|^2) + \frac{1}{4\delta t}\Big(\|\boldsymbol{u}^{n+1}\|^2 - \|\boldsymbol{u}^n\|^2$$

$$+ \|2\boldsymbol{u}^{n+1} - \boldsymbol{u}^n\|^2 - \|2\boldsymbol{u}^n - \boldsymbol{u}^{n-1}\|^2 + \|\boldsymbol{u}^{n+1} - 2\boldsymbol{u}^n + \boldsymbol{u}^{n-1}\|^2\Big).$$

For the projection step, we rewrite (3.17) as

(3.64)
$$\frac{3}{2\delta t}\boldsymbol{u}^{n+1} + \nabla p^{n+1} = \frac{3}{2\delta t}\widetilde{\boldsymbol{u}}^{n+1} + \nabla p^n.$$

By squaring both sides of the above equality, we obtain

(3.65)
$$\frac{9}{4\delta t^2}\|\boldsymbol{u}^{n+1}\|^2 + \|\nabla p^{n+1}\|^2 = \frac{9}{4\delta t^2}\|\widetilde{\boldsymbol{u}}^{n+1}\|^2 + \|\nabla p^n\|^2 + \frac{3}{\delta t}(\widetilde{\boldsymbol{u}}^{n+1}, \nabla p^n),$$

namely, we have

(3.66)
$$\frac{3}{4\delta t}(\|\boldsymbol{u}^{n+1}\|^2 - \|\widetilde{\boldsymbol{u}}^{n+1}\|^2) + \frac{\delta t}{3}(\|\nabla p^{n+1}\|^2 - \|\nabla p^n\|^2) = (\widetilde{\boldsymbol{u}}^{n+1}, \nabla p^n).$$

By taking the L^2 inner product of (3.48) with $\boldsymbol{u}^{n+1}$, we have

(3.67)
$$\frac{3}{4\delta t}\Big(\|\boldsymbol{u}^{n+1}\|^2 - \|\widetilde{\boldsymbol{u}}^{n+1}\|^2 + \|\boldsymbol{u}^{n+1} - \widetilde{\boldsymbol{u}}^{n+1}\|^2\Big) = 0.$$

Finally, by combining (3.56), (3.57), (3.60), (3.61), (3.63), (3.66) and (3.67), we obtain

$$\frac{1}{M}\|\dot{\phi}^{n+1}\|^2 + \frac{3}{4\delta t}\|\boldsymbol{u}^{n+1} - \widetilde{\boldsymbol{u}}^{n+1}\|^2 + \frac{\delta t}{3}(\|\nabla p^{n+1}\|^2 - \|\nabla p^n\|^2)$$

$$+ \frac{K}{4\delta t}\Big(\|\psi^{n+1}\|^2 - \|\psi^n\|^2 + \|2\psi^{n+1} - \psi^n\|^2 - \|2\psi^n - \psi^{n-1}\|^2 + \|\psi^{n+1} - 2\psi^n + \psi^{n-1}\|^2\Big)$$

$$+ \frac{K}{8\epsilon^2\delta t}\Big(\|U^{n+1}\|^2 - \|U^n\|^2 + \|2U^{n+1} - U^n\|^2 - \|2U^n - U^{n-1}\|^2 + \|U^{n+1} - 2U^n + U^{n-1}\|^2\Big)$$

$$+ \frac{1}{4\delta t}\Big(\|\boldsymbol{u}^{n+1}\|^2 - \|\boldsymbol{u}^n\|^2 + \|2\boldsymbol{u}^{n+1} - \boldsymbol{u}^n\|^2 - \|2\boldsymbol{u}^n - \boldsymbol{u}^{n-1}\|^2 + \|\boldsymbol{u}^{n+1} - 2\boldsymbol{u}^n + \boldsymbol{u}^{n-1}\|^2\Big)$$

$$+ (\sigma(\widetilde{\boldsymbol{u}}^{n+1}, \nabla\phi^{*,n+1}), \nabla\widetilde{\boldsymbol{u}}^{n+1}) = 0,$$

that concludes the theorem. □

Remark 3.6. *Heuristically, the $\frac{1}{\delta t}(E_{tot-bdf2}^{n+1} - E_{tot-bdf2}^n)$ is a second order approximation of $\frac{d}{dt}E(\phi, U)$ at $t = t^{n+1}$. For instance, for any smooth variable S with time, one can write*

$$\Big(\frac{\|S^{n+1}\|^2 + \|2S^{n+1} - S^n\|^2}{2\delta t}\Big) - \Big(\frac{\|S^n\|^2 + \|2S^n - S^{n-1}\|^2}{2\delta t}\Big)$$

$$\cong \Big(\frac{\|S^{n+2}\|^2 - \|S^n\|^2}{2\delta t}\Big) + O(\delta t^2) \cong \frac{d}{dt}\|S(t^{n+1})\|^2 + O(\delta t^2).$$

Remark 3.7. *Although we consider only time discrete schemes in this paper, the results here can be carried over to any consistent finite-dimensional Galerkin type approximations since the analyses are based on the variational formulation with all test functions in the same space as the space of the trial functions. The details for the fully discrete scheme will be left to the interested readers.*

Remark 3.8. *For the numerical schemes proposed in this paper, the energy stability is formally derived. The error estimates for the second order scheme for the layer variable is straightforward when the velocity field is null. This is because the H^2 bound exists for ϕ from the Poincaré inequality, and the corresponding convergence analysis can be further carried out. For the hydrodynamics coupled model, we have combine the analysis work for the projection method, see [53, 64], and follow the same lines as [19] to handle the nonlinear convective and stress terms where the basic tool is to use sobolev embeddings among various Banach spaces. We will implement the rigorous error analysis in the future work.*

4. Numerical simulations

We now present various numerical experiments to validate the theoretical results derived in the previous sections and demonstrate the stability and accuracy of the proposed numerical schemes. In all examples, we use the inf-sup stable Iso-$P2/P1$ element [61] for the velocity and pressure, and linear element for the phase function ϕ and ψ. As for as the stable element for the Navier-Stokes variables (u, p), one can read the related literatures in [32–35, 40]. If not explicit specified, the model parameters take default values given below:

$$(4.1) \qquad \epsilon = 0.05, \mu_4 = 0.02, \mu_1 = \mu_5 = 0, M = 1 \times 10^{-6}, K = 0.01.$$

4.1. **Accuracy test.** We first perform numerical simulations to test the convergence rates of the two proposed schemes (3.11)-(3.18) (denoted by CN2), and (3.42)-(3.49) (denoted by BDF2).

δt	Error_u	Order	Error_v	Order	Error_p	Order	Error_ϕ	Order
1×10^{-2}	4.61×10^{-4}	–	4.75×10^{-4}	–	1.18×10^{-1}	–	1.81×10^{-4}	–
5×10^{-3}	1.15×10^{-4}	2.003	1.19×10^{-4}	1.997	5.87×10^{-2}	1.007	4.53×10^{-5}	1.998
2.5×10^{-3}	2.88×10^{-5}	1.997	2.97×10^{-5}	2.002	2.94×10^{-2}	0.997	1.13×10^{-5}	2.003
1.25×10^{-3}	7.21×10^{-6}	1.998	7.43×10^{-6}	1.999	1.47×10^{-2}	1.000	2.83×10^{-6}	1.997
6.25×10^{-4}	1.80×10^{-6}	2.002	1.86×10^{-6}	1.998	7.30×10^{-3}	1.009	7.08×10^{-7}	1.999

TABLE 1. The L^2 errors for the velocity field $\boldsymbol{u} = (u, v)$, the phase variable ϕ and the pressure p at $t = 1$ for by the scheme CN2 using different temporal resolutions with the exact solution of (4.2).

δt	Error$_u$	Order	Error$_v$	Order	Error$_p$	Order	Error$_\phi$	Order
1×10^{-2}	4.00×10^{-3}	–	4.12×10^{-3}	–	3.92×10^{-1}	–	1.57×10^{-3}	–
5×10^{-3}	9.62×10^{-4}	2.055	9.91×10^{-4}	2.055	1.96×10^{-1}	1.000	3.78×10^{-4}	2.054
2.5×10^{-3}	2.36×10^{-4}	2.027	2.43×10^{-4}	2.027	9.92×10^{-2}	0.982	9.26×10^{-5}	2.029
1.25×10^{-3}	5.83×10^{-5}	2.017	6.00×10^{-5}	2.017	4.91×10^{-2}	1.014	2.29×10^{-5}	2.015
6.25×10^{-4}	1.45×10^{-5}	2.007	1.49×10^{-5}	2.009	2.46×10^{-2}	0.997	5.69×10^{-6}	2.008

TABLE 2. The L^2 errors for the velocity field $\boldsymbol{u} = (u, v)$, the phase variable ϕ and the pressure p at $t = 1$ for by the scheme BDF2 using different temporal resolutions with the exact solution of (4.2).

δt	Error$_u$	Order	Error$_v$	Order	Error$_p$	Order	Error$_\phi$	Order
1×10^{-2}	4.61×10^{-4}	–	4.75×10^{-4}	–	1.18×10^{-1}	–	2.01×10^{-4}	–
5×10^{-3}	1.18×10^{-4}	1.966	1.21×10^{-4}	1.972	5.87×10^{-2}	1.007	5.12×10^{-5}	1.973
2.5×10^{-3}	3.12×10^{-5}	1.919	3.21×10^{-5}	1.914	2.94×10^{-2}	0.997	1.23×10^{-5}	2.057
1.25×10^{-3}	8.14×10^{-6}	1.938	8.21×10^{-6}	1.967	1.47×10^{-2}	1.000	2.97×10^{-6}	2.050
6.25×10^{-4}	2.09×10^{-6}	1.961	2.16×10^{-6}	1.926	7.33×10^{-3}	1.003	7.92×10^{-7}	1.901

TABLE 3. The L^2 numerical errors at $t = 1$ that are computed by the scheme CN2 using various temporal resolutions with the initial conditions of (4.3), for mesh refinement test in time.

δt	Error$_u$	Order	Error$_v$	Order	Error$_p$	Order	Error$_\phi$	Order
1×10^{-2}	4.00×10^{-3}	–	4.12×10^{-3}	–	3.93×10^{-1}	–	1.56×10^{-3}	–
5×10^{-3}	9.64×10^{-4}	2.052	9.93×10^{-4}	2.052	1.96×10^{-1}	1.003	3.71×10^{-4}	2.072
2.5×10^{-3}	2.39×10^{-4}	2.012	2.46×10^{-4}	2.013	9.82×10^{-2}	0.997	9.95×10^{-5}	1.898
1.25×10^{-3}	5.74×10^{-5}	2.057	5.94×10^{-5}	2.050	4.91×10^{-2}	1.000	2.60×10^{-5}	1.936
6.25×10^{-4}	1.49×10^{-5}	1.945	1.57×10^{-5}	1.919	2.46×10^{-2}	0.997	6.42×10^{-6}	2.017

TABLE 4. The L^2 numerical errors at $t = 1$ that are computed by the scheme BDF2 using various temporal resolutions with the initial conditions of (4.3), for mesh refinement test in time.

4.1.1. *Presumed exact solution.* In the first example, we set the computed domain to be $\Omega = [0, 2]^2$ and assume the following functions

$$(4.2) \quad \begin{cases} u(t, x, y) = \pi \sin(2\pi y) \sin^2(\pi x) \sin t, \\ v(t, x, y) = -\pi \sin(2\pi x) \sin^2(\pi y) \sin t, \\ \phi(t, x, y) = 2 + \cos(\pi x) \cos(\pi y) \sin t, \\ p(t, x, y) = \cos(\pi x) \sin(\pi y) \sin t \end{cases}$$

to be the exact solution, and impose some suitable force fields such that the given solution can satisfy the system. We use 10145 nodes and 19968 triangle elements for the discretization of the space. In Table 1 and 2, we list the L^2 errors of the velocity field $\boldsymbol{u} = (u, v)$, the phase variable ϕ and the pressure p between the numerically simulated solution and the exact solution at $t = 1$ with different time step sizes, for the schemes CN2 and BDF2, respectively. We observe that the schemes CN2 and BDF2 achieve almost perfect second order accuracy for $\boldsymbol{u}$ and ϕ, and first order accuracy for p in time as expected, respectively.

4.1.2. *Mesh refinement in time.* We now perform more refinement tests for temporal convergence. We set the initial conditions as follows,

$$(4.3) \qquad \phi_0 = 2, \ \boldsymbol{u}_0 = (u_0, v_0) = 0, \ p_0 = 0.$$

We perform the refinement test of the time step size. Since the exact solutions are not known, we choose the solution obtained by the scheme CN2 with the time step size $\delta t = 1 \times 10^{-6}$ as the benchmark solution for computing errors. We present the L^2 of the variables between the numerical solution and the exact solution at $t = 1$ with different time step sizes in Table 3 and Table 4 for the schemes CN2 and BDF2, respectively. As the previous tests, we observe that the schemes CN2 and BDF2 achieve almost perfect second order accuracy for $\boldsymbol{u}$ and ϕ, and the first order accuracy for p, respectively.

4.2. **Layer motion.** In this example, we consider the layer motion using the second order scheme CN2. The following initial conditions are taken as follows,

$$(4.4) \qquad \phi_0 = \sin x \cos^2 y, \boldsymbol{u}_0 = (u_0, v_0) = 0, p_0 = 0,$$

that had been studied in [30]. We set the computed domain to be $\Omega = [-1, 1]^2$ and the space is discretized by using 10145 nodes and 19968 triangle elements. The model parameters are from (4.1).

We emphasize that any time step size δt is allowable for the computations from the stability concern since all developed schemes are unconditionally energy stable. But larger time step will definitely induce large numerical errors. Therefore, we need to discover the rough range of the allowable maximum time step size in order to obtain good accuracy and to consume as low computational cost as possible. This time step range could be estimated through the energy evolution curve plots, shown in Fig. 1, where we compare the time evolution of the free energy for five different time step sizes until $t = 200$ using the second order scheme CN2. We observe that all five energy curves show decays monotonically for all time step sizes, which numerically confirms that our algorithms are unconditionally energy stable. For smaller time steps of $\delta t = 0.0001, 0.0005, 0.001, 0.005, 0.01$, all five energy curves coincide very well, that means we can just use the maximum allowable time step $\delta t = 0.01$ without worrying the accuracy.

In Fig. 2 and Fig. 3, we show the dynamical evolution of the layer function ϕ, and the velocity field $\boldsymbol{u}$ until the simulation reaches the steady state, respectively. The obtained results show qualitatively consistent features with the numerical examples in [30].

4.3. **Layer undulation under shear flow.** In this example, we consider the numerical simulations of the layer undulation under shear flow using the second order scheme CN2. We set the computed domain to be $\Omega = [-1, 1] \times [-0.5, 0.5]$ and the space is discretized by using 10145 nodes and 19968 triangle elements. The initial condition reads as follows:

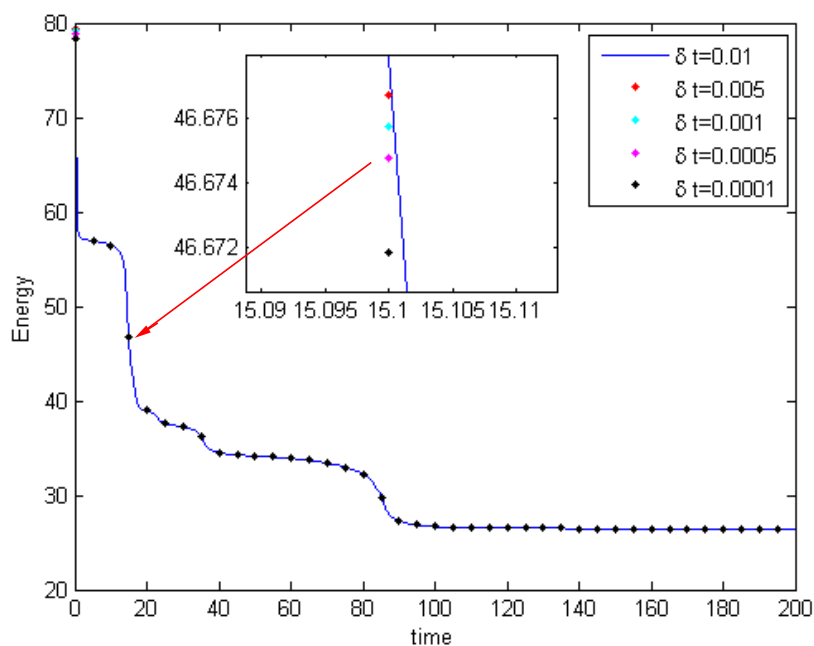$$(4.5) \qquad \phi_0 = y, \boldsymbol{u}_0 = (0.4y, 0), p_0 = 0,$$

FIG. 1. Time evolution of the free energy functional till $t = 200$ for five different time steps of $\delta t = 0.01$, 0.005, 0.001, 0.0005, and 0.0001 using the scheme CN2. The energy curves show the decays for all time steps, which confirms that our algorithm is unconditionally stable. The small differences in the energy evolution for all five time steps are shown as well.
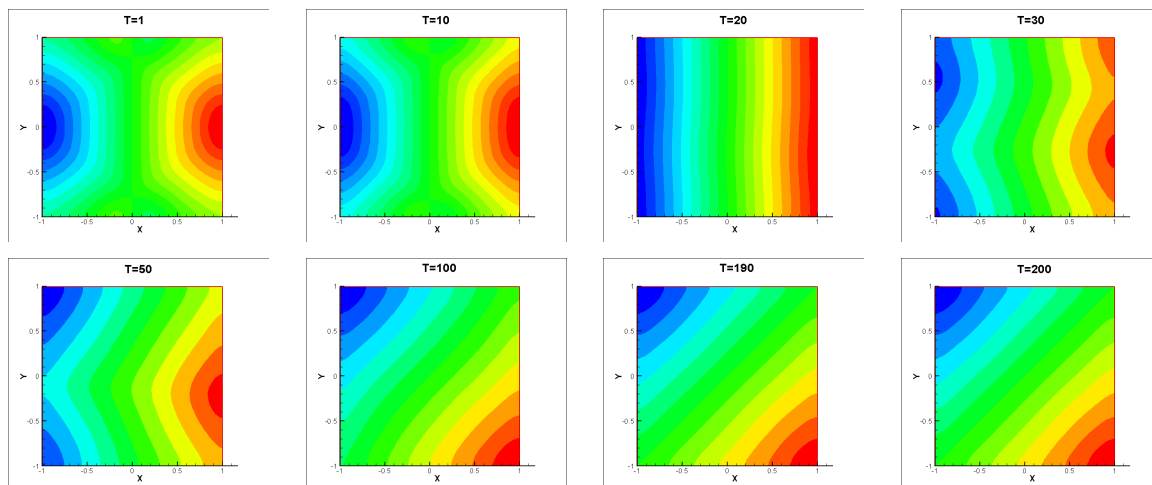

FIG. 2. The dynamical evolution of the layer function ϕ for the layer motion example with the time step $\delta t = 0.01$. Snapshots of the numerical approximation are taken at $t = 1$, 10, 20, 30. 50, 100, 190, and 200.
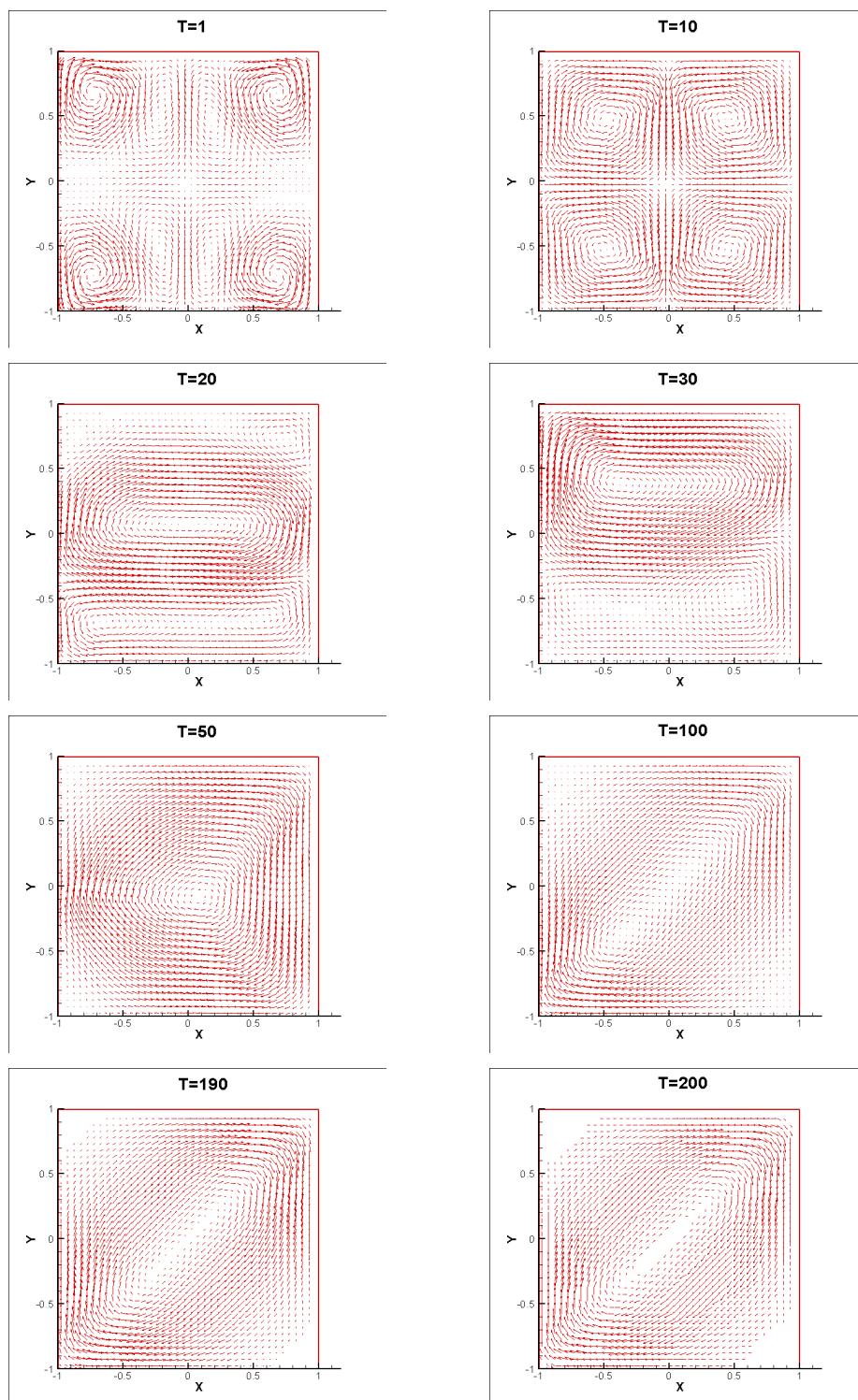
FIG. 3. *The profiles of the velocity field $\boldsymbol{u}$ for the layer motion example with the time step $\delta t = 0.01$. Snapshots of the numerical approximation of $\boldsymbol{u}$ are taken at $t = 1$, 10, 20, 30. 50, 100, 190, and 200.*
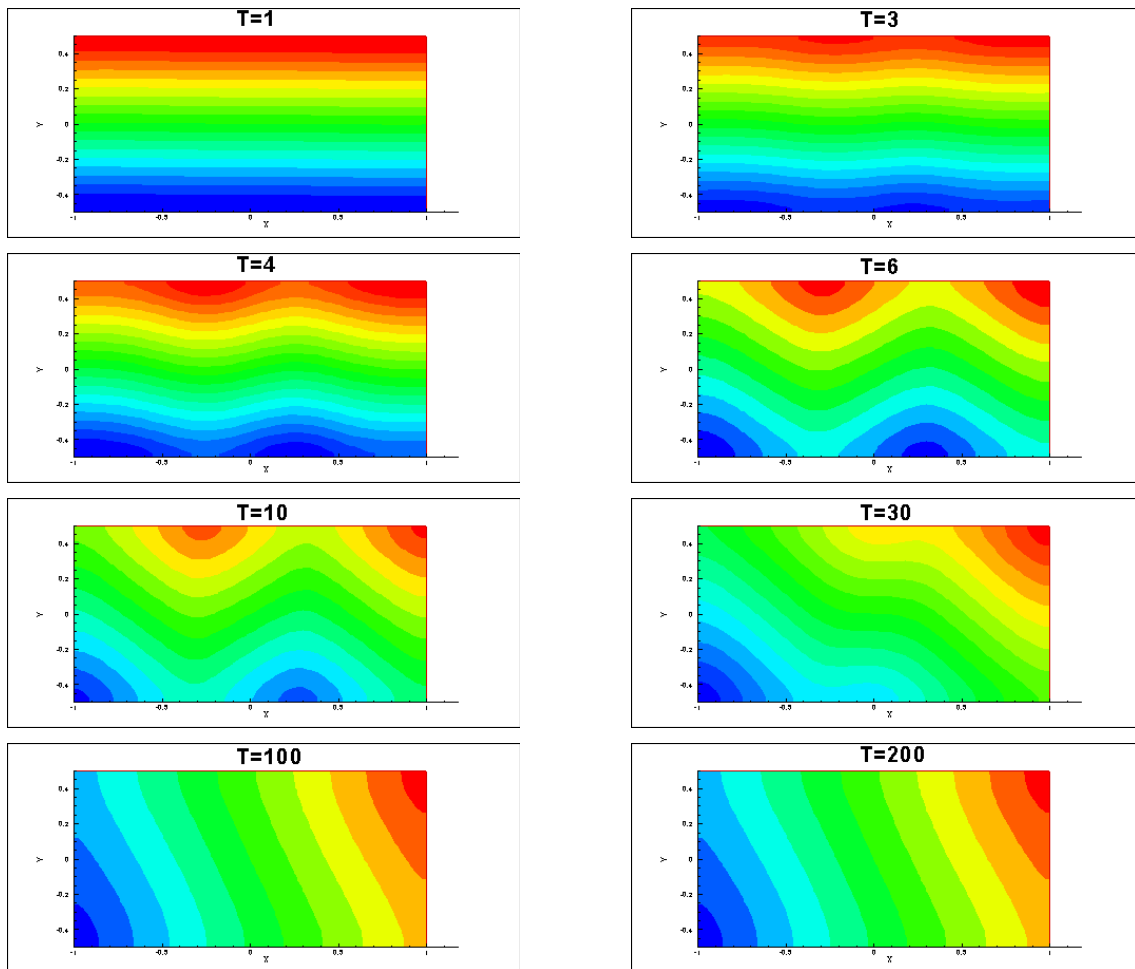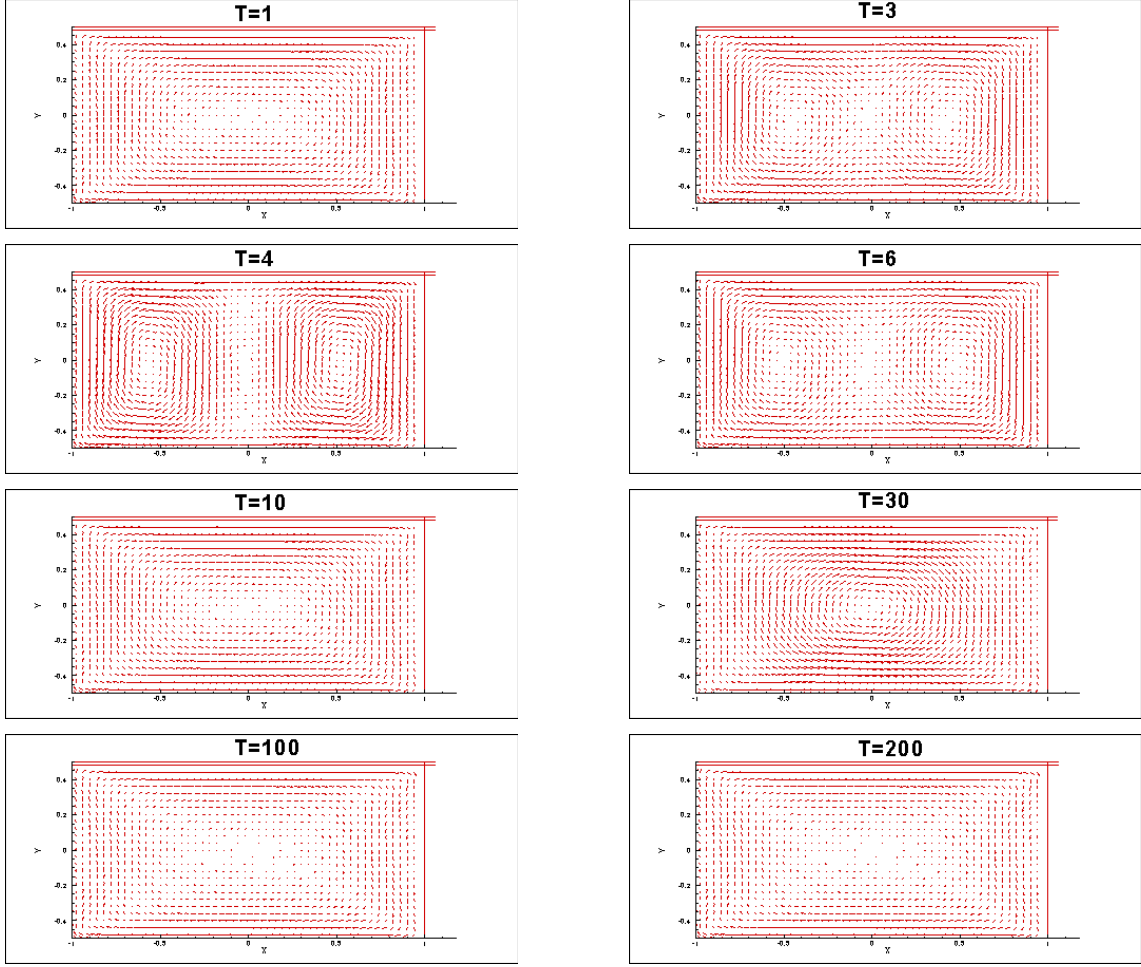
FIG. 4. The dynamical evolution of the layer function ϕ for the layer undulations under the shear flow with the time step $\delta t = 0.01$. Snapshots of the numerical approximation are taken at $t = 1, 3, 4, 6, 10, 30, 100, 200$.

and the boundary condition for the velocity field are set to be

(4.6) $$\boldsymbol{u}|_{y=0.5} = (0.2, 0), \ \boldsymbol{u}|_{y=-0.5} = (-0.2, 0), \ \boldsymbol{u}|_{x=\pm 1} = (0, 0).$$

The model parameters are still from (4.1).

In Fig. 4 and Fig. 5, we show the dynamical evolution of the layer function ϕ, and the velocity field $\boldsymbol{u}$ until the simulation reaches the steady state, respectively. The obtained profiles of undulational layers are consistent with the theoretical results predicted in [48] and the numerical results using the molecular dynamics approach in [60].

4.4. **The sawtooth feature under external magnetic field.** Applying an external magnetic field is one of the most efficient approach to control and produce various nano-structured materials, and had been well-studied in a number of experimental, modeling and numerical literatures, see [25, 27, 49, 51]. In the last numerical example, we consider the dynamical behaviors of the smectic-A

FIG. 5. The dynamical evolution of the velocity field $\boldsymbol{u}$ for the layer undulations under the shear flow with the time step $\delta t = 0.01$. Snapshots of the numerical approximation are taken at $t = 1, 3, 4, 6, 10, 30, 100, 200$.

LCs in the presence of an applied magnetic field. When an external magnetic filed is applied, an additional term contributed by it is added to the free energy of the model system, that reads as

$$(4.7) \qquad E(\phi, \boldsymbol{u}) = \int_\Omega \Big(\frac{1}{2}|\boldsymbol{u}|^2 + \frac{K}{2}|\Delta\phi|^2 + K\frac{(|\nabla\phi|^2 - 1)^2}{4\epsilon^2} - \tau(\nabla\phi \cdot \boldsymbol{h})^2 \Big) d\boldsymbol{x},$$

where $\boldsymbol{h}$ is a given unit vector representing the direction of the magnetic field, and τ is a nonnegative parameter denoting the strength of the applied magnetic field.

Thus the new equation for the layer function ϕ reads as follows

$$(4.8) \qquad \phi_t + \nabla \cdot (\boldsymbol{u}\phi) = -Mw,$$

$$(4.9) \qquad w = \frac{\delta E}{\delta\phi} = K(\Delta^2\phi - \frac{1}{\epsilon^2}\nabla \cdot (|\nabla\phi|^2 - 1)\nabla\phi)) + \tau\nabla \cdot (\nabla\phi \cdot \boldsymbol{h})\boldsymbol{h},$$
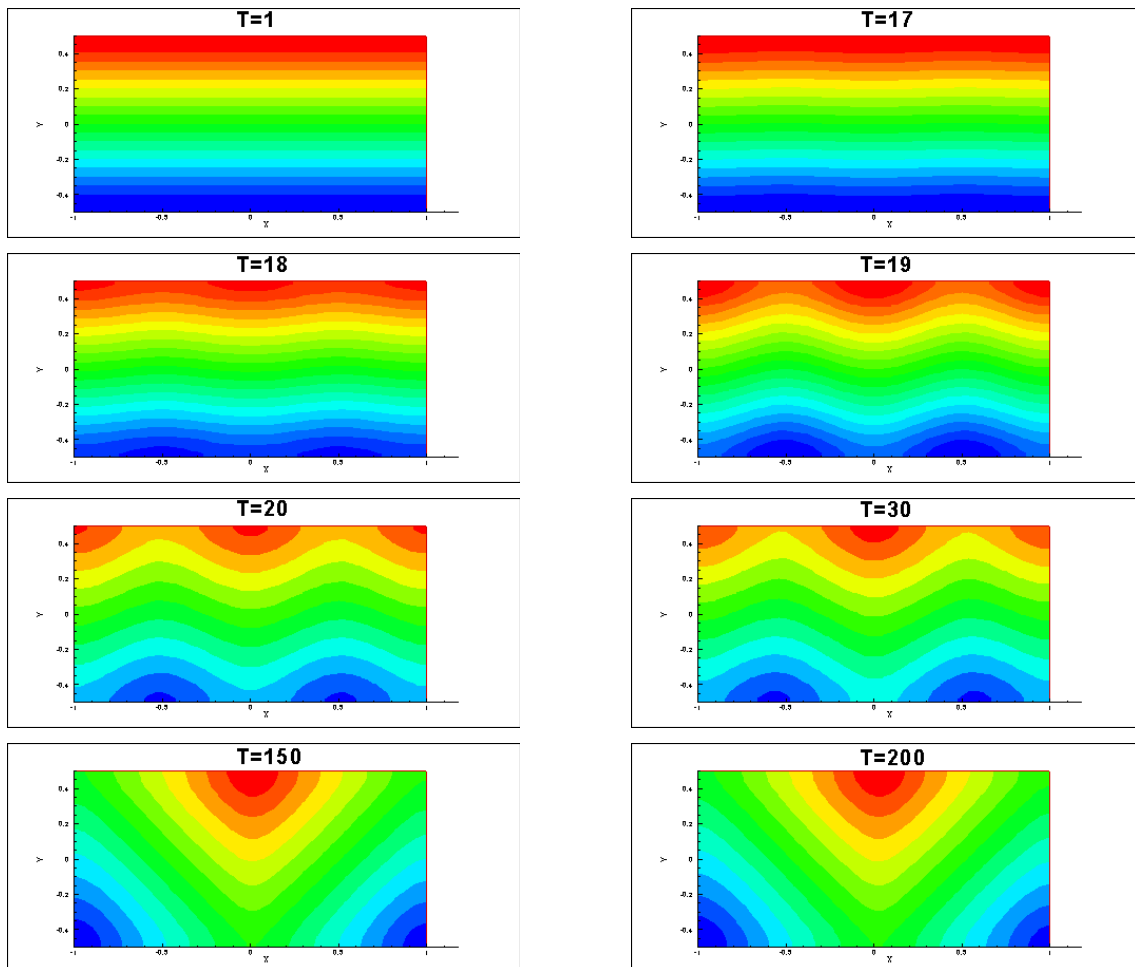
FIG. 6. The dynamical evolution of the layer function ϕ under external the magnetic field with the time step $\delta t = 0.01$. Snapshots of the numerical approximation are taken at $t = 1, 17, 18, 19, 20, 30, 150, 200$.

and the equations for the fluid velocity are still (2.7)-(2.8). The magnetic field term can be viewed as an imposed external force, i.e., we treat this term by the second order extrapolations.

We let $\boldsymbol{h} = (1, 0)$ and $\tau = 10$ and choose the same initial conditions, computed domain and the space discretizations as the previous shear flow example. In Fig. 6, we present that the dynamical motion of the layer variable ϕ, the undulation profile is formed from $t = 2.1$ to $t = 3$. This sawtooth feature is qualitatively consistent with the numerical simulation in [27] using the de Gennes' smectic-A model. The final equilibrium solution is obtained after $t = 150$. We present the snapshots of the velocity field in Fig. 7 as well.

5. Conclusions and remarks

In this paper, we have constructed a set of efficient numerical schemes for solving the hydrodynamics coupled smectic-A LCs model. The schemes are (i) second order accurate in time; (ii)
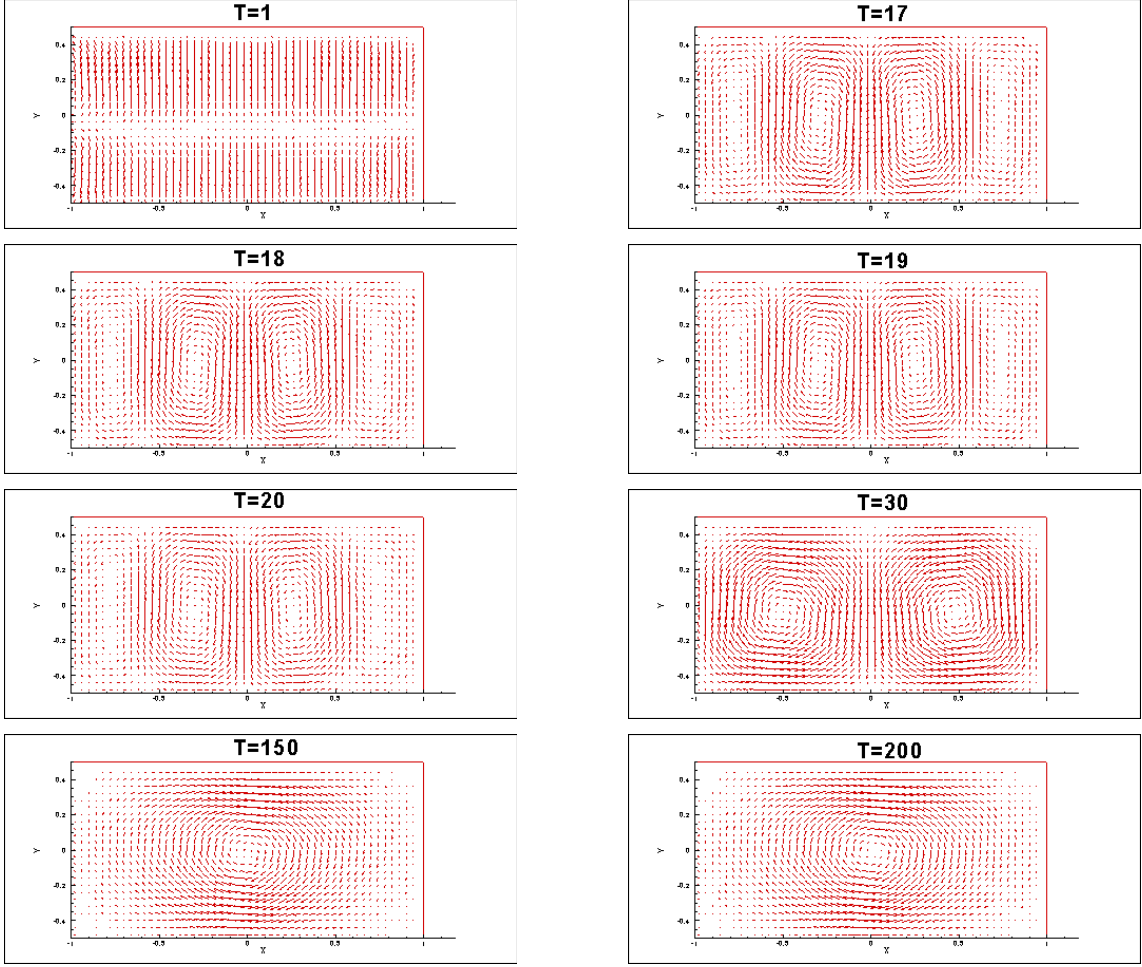
FIG. 7. The dynamical evolution of the velocity field $\boldsymbol{u}$ under external the magnetic field with the time step $\delta t = 0.01$. Snapshots of the numerical approximation are taken at $t = 1, 17, 18, 19, 20, 30, 150, 200$.

unconditional energy stable; and (iii) linear and easy to implement. Various numerical results are presented to validate the accuracy of our schemes. We have also presented a number of numerical simulations to show the morphological evolutions, in particular, the layer undulation under shear flow as well as the sawtooth profile induced by the external magnetic field.

<h2 align="center">REFERENCES</h2>

[1] S. Badia, F. Guillen Gonzalez, and J. V. Gutierrez-Santacreu. An overview on numerical analyses of nematic liquid crystal flows. *Arch. Comput. Meth. Eng.*, 18(3):285–313, 2011.

[2] F. Bethue, H. Brezis, and F. Helein. Asymptotics for the minimization of a ginzburg-landau functional. *Calc. Var.*, 1:123–148, 1993.

[3] D. Brogioli and A. Vailati. Diffusive mass transfer by nonequilibrium fluctuations: Fick's law revisited. *Phys. Rev. E*, 63:012105, 2000.

[4] J. W. Cahn and J. E. Hillard. Free energy of a nonuniform system. I. Interfacial free energy. *J. Chem. Phys.*, 28:258–267, 1958.

[5] M. C. Calderer and S. Joo. A continuum theory of chiral smectic C liquid crystals. *SIAM J. Appl. Math.*, 69(3):787–809, 2008.

[6] S. Chandrasekhar. *Liquid crystals*, volume 1. Cambridge University Press, 2nd edition, 1992.

[7] J. Chen and T.C. Lubensky. Landau-ginzburg mean-field theory for the nematic-c and nematic to smectic-a phase transitions. *Phys. Rev. A.*, 14(3):1202–1207, 1976.

[8] R. Chen, G. Ji, X. Yang, and H. Zhang. Decoupled energy stable schemes for phase-field vesicle membrane model. *J. Comput. Phys.*, 302:509–523, 2015.

[9] Q. Cheng, X. Yang, and J. Shen. Efficient and accurate numerical schemes for a hydrodynamically coupled phase field diblock copolymer model. *J. Comput. Phys.*, 341:44–60, 2017.

[10] B. Climent-Ezquerra and F. Guillén-González. Global in time solution and time-periodicity for a smectic-a liquid crystal model. *Commun. Pure Appl. Anal.*, 9(6):1473–1493, 2010.

[11] B. Climent-Ezquerra and F. Guillén-González. A review of mathematical analysis of nematic and smectic-a liquid crystal models. *Euro. J. Appl. Math.*, 25(1):133–153, 2014.

[12] T. A. Davis and E. C. Gartland. Finite element analysis of the landau-de gennes minimization problem for liquid crystals. *SIAM J. Numer. Anal.*, 35:336–362, 1998.

[13] P. G. de Gennes and J. Prost. *The physics of liquid crystals.* Oxford Science, 1993.

[14] W. E. Nonlinear continuum theory of smectic-a liquid crystal. *Arch. Rat. Mech. Anal.*, 137(2):1159–175, 1997.

[15] W. E and J-G. Liu. Projection method. I. Convergence and numerical boundary layers. *SIAM J. Numer. Anal.*, 32(4):1017–1057, 1995.

[16] J. L. Ericksen. Anisotropic fluids. *Archive for Rational Mechanics and Analysis*, 4:231–237, 1960.

[17] J. L. Ericksen. Hydrostatic theory of liquid crystal. *Archive for Rational Mechanics and Analysis*, 9:371–378, 1962.

[18] D. J. Eyre. Unconditionally gradient stable time marching the Cahn-Hilliard equation. In *Computational and mathematical models of microstructural evolution (San Francisco, CA, 1998)*, volume 529 of *Mater. Res. Soc. Sympos. Proc.*, pages 39–46. MRS, Warrendale, PA, 1998.

[19] X. Feng, Y. He, and C. Liu. Analysis of finite element approximations of a phase field model for two-phase fluids. *Mathematics of Computation*, 76(258):539–571, 2007.

[20] X. Feng and A. Prol. Numerical analysis of the allen-cahn equation and approximation for mean curvature flows. *Numer. Math.*, 94:33–65, 2003.

[21] M. G. Forest, S. Heidenreich, S. Hess, X. Yang, and R. Zhou. Robustness of pulsating jet-like layers in sheared nano-rod dispersions. *J. Non-Newtonian Fluid Mech.*, 155:130–145, 2008.

[22] M. G. Forest, S. Heidenreich, S. Hess, X. Yang, and R. Zhou. Dynamic texture scaling of sheared nematic polymers in the large Ericksen number limit. *J. Non-Newtonian Fluid Mech.*, 165:687–697, 2010.

[23] M. G. Forest, Q. Wang, and X. Yang. Lcp droplet dispersions: a two-phase, diffuse-interface kinetic theory and global droplet defect predictions,. *Soft Matter*, 37:9642–9660, 2012.

[24] C. J. García-Cervera, T. Giorgi, and S. Joo. The phase transitions from chiral nematic toward smectic liquid crystals. *Commun. Math. Phys.*, 269(2):367–399, 2007.

[25] C. J. García-Cervera, T. Giorgi, and S. Joo. Sawtooth profile in smectic a liquid crystals. *SIAM J. Appl. Math.*, 76(1):217–237, 2016.

[26] C. J. García-Cervera and S. Joo. Layer undulations in smectic a liquid crystals. *J. Comput. Theor. Nanosci.*, 7(4):1–7, 2010.

[27] C. J. García-Cervera and S. Joo. Analytic description of layer undulations in smectic a liquid crystals. *Arch. Rational Mech. Anal. 203*, 203:1–43, 2012.

[28] J. L. Guermond, P. Minev, and J. Shen. An overview of projection methods for incompressible flows. *Comput. Methods Appl. Mech. Engrg.*, 195:6011–6045, 2006.

[29] J. L. Guermond, J. Shen, and X. Yang. Error analysis of fully discrete velocitycorrection methods for incompressible flows. *Math. Comp.*, 77:1387–1405, 2008.

[30] F. Guillén-González and G. Tierra. Approximation of smectic-a liquid crystals. *Comput. Methods Appl. Mech. Engrg.*, 290:342–361, 2015.

[31] F. Guillén-González and G. Tierra. On linear schemes for a Cahn-Hilliard diffuse interface model. *J. Comput. Phys.*, 234:140–171, 2013.

[32] Y. He. The euler implicit/explicit scheme for the 2d time-dependent navier-stokes equations with smooth or non-smooth initial data. *Math. Comp.*, 77:2097–2124, 2008.

[33] Y. He and J. Li. A stabilized finite element method based on local polynomial pressure projection for the stationary navier-stokes equations. *Appl. Numer. Math.*, 58:1503–1514, 2008.

[34] Y. He, Y. Liu, and T. Tang. On large time-stepping methods for the cahn-hilliard equation. *Appl. Numer. Math.*, 57:616–628, 2007.

[35] Y. He and W. Sun. Stability and convergence of the crank-nicolson/adams-bashforth scheme for the time-dependent navier-stokes equations. *SIAM J. Numer. Anal.*, 45:837–869, 2007.

[36] R. Ingram. A new linearly extrapolated Crank-Nicolson time-stepping scheme for the Navier-Stokes equations. *Math. Comp.*, 82(284):1953–1973, 2013.

[37] D. H. Klein, C. J. Garcia-Cervera, H. D. Ceniceros, and L. G. Leal. Ericksen number and deborah number cascade predictions of a model for liquid crystalline polymers for simple shear flow. *Phys. Fluids*, 19:023101, 2007.

[38] F. M. Leslie. Some constitutive equations for liquid crystals. *Archive for Rational Mechanics and Analysis*, 28:265–283, 1968.

[39] F. M. Leslie, I. W. Stewart, and M. Nakagawa. A continuum theory for smectic c liquid crystals. *Molecular Crystals and Liquid Crystals*, 198(1):443–454, 1991.

[40] J. Li and Y. He. A stabilized finite element method based on two local gauss integrations for the stokes equations. *J. Comput. Appl. Math.*, 214:58–65, 2008.

[41] F. H. Lin. On nematic liquid crystals with variable degree of orientation. *Communications on Pure and Applied Mathematics*, 44:453–468, 1991.

[42] P. Lin and C. Liu. Simulations of singularity dynamics in liquid crystal flows: a C^0 finite element approach. *J. Comput. Phys.*, 215(1):348–362, 2006.

[43] C. Liu. The dynamic for incompressible smectic-a liquid crystal: existence and regularity. *Discrete Contin. Dyn. Syst.*, 6(3):591–608, 2000.

[44] C. Liu and J. Shen. A phase field model for the mixture of two incompressible fluids and its approximation by a Fourier-spectral method. *Physica D*, 179(3-4):211–228, 2003.

[45] C. Liu, J. Shen, and X. Yang. Dynamics of defect motion in nematic liquid crystal flow: modeling and numerical simulation. *Comm. Comput. Phys*, 2:1184–1198, 2007.

[46] C. Liu and N. J. Walkington. Approximation of liquid crystal flows. *SIAM J. Numer. Anal.*, 37:725–741, 2000.

[47] C. S. MacDonald, J. A. Mackenzie, and A. Ramage. Efficient moving mesh method for q-tensor models of nematic liquid crystals. *SIAM J. Sci. Comput.*, 37(2):215–238, 2015.

[48] P. Oswald and S. I. Ben-Abraham. Undulation instability under shear in smectic a liquid crystals. *J. de Physique*, 43(8):1193–1197, 1982.

[49] A. M. Parshin, V. A. Gunyakov, V. Y. Zyryanov, and V. F. Shabanov. Electric and magnetic field-assisted orientational transitions in the ensembles of domains in a nematic liquid crystal on the polymer surface. *Inter. J. Molecular Sci.*, 15(10):17838–17851, 2014.

[50] A. D. Rey. Capillary models for liquid crystal fibers membranes, films, and drops. *Soft Matter*, 3(3):1349–1368, 2007.

[51] A. Sakamoto, K. Yoshino, U. Kubo, and Y. Inuishi. Effects of the magnetic field on the phase transition temperature between smectic-a and nematic states. *Japanese Journal of Applied Physics*, 15(3):545, 1976.

[52] A. Segatti and H. Wu. Finite dimensional reduction and convergence to equilibrium for incompressible smectic-a liquid crystal flows. *SIAM J. Math. Anal.*, 43(6):2445–2481, 2011.

[53] J. Shen. On error estimates of the projection methods for the Navier-Stokes equations: second-order schemes. *Math. Comp.*, 65(215):1039–1065, 1996.

[54] J. Shen and X. Yang. An efficient moving mesh spectral method for the phase-field model of two-phase flows. *J. Comput. Phys.*, 228:2978–2992, 2009.

[55] J. Shen and X. Yang. Numerical approximations of Allen-Cahn and Cahn-Hilliard equations. *Disc. Conti. Dyn. Sys.-A*, 28:1669–1691, 2010.

[56] J. Shen and X. Yang. A phase field model and its numerical approximation for two phase incompressible flows with different densities and viscosities. *SIAM J. Sci. Comput.*, 32(3):1159–1179, 2010.

[57] J. Shen and X. Yang. Decoupled energy stable schemes for phase filed models of two phase complex fluids. *SIAM J. Sci. Comput.*, 36:B122–B145, 2014.

[58] J. Shen and X. Yang. Decoupled energy stable schemes for phase field models of two phase incompressible flows. *SIAM J. Num. Anal.*, 53(1):279–296, 2015.

[59] J. Shen, X. Yang, and H. Yu. Efficient energy stable numerical schemes for a phase field moving contact line model. *J. Comput. Phys.*, 284:617–630, 2015.

[60] Th. Soddemann, G.K. Auernhammer, H. Guo, B. Dunweg, and K. Kremer. Shear-induced undulation of smectic-a: Molecular dynamics simulations vs. analytical theory. *Eur. Phys. J. E*, 13:141–151, 2004.

[61] M. Tabata and D. Tagamai. Error estimates for finite element approximations of drag and lift in nonstationary navier-stokes flows. *Jpn. J. Ind. Appl. Math.*, 17(3):371–389, 2000.

[62] R. Temam. *Navier-Stokes equations: Theory and numerical analysis*. American Mathematical Society, 2001.

[63] G. Tierra and F. Guillén-González. Numerical methods for solving the Cahn-Hilliard equation and its applicability to related energy-based models. *Arch. Comput. Methods Eng.*, 22:269–289, 2015.

[64] J. van Kan. A second-order accurate pressure-correction scheme for viscous incompressible flow. *SIAM J. Sci. Statist. Comput.*, 7(3):870–891, 1986.

[65] C. Xu and T. Tang. Stability analysis of large time-stepping methods for epitaxial growth models. *SIAM. J. Num. Anal.*, 44:1759–1779, 2006.

[66] K. Xu, M. G. Forest, and X. Yang. Shearing the I-N phase transition of liquid crystalline polymers: long-time memory of defect initial data. *Disc. Conti. Dyn. Sys.-B*, 15:457–474, 2010.

[67] X. Xu, G. J. Van Zwieten, and K. G. van der Zee. Stabilized second-order convex splitting schemes for Cahn-Hilliard models with application to diffuse-interface tumor-growth models. *Inter. J. Num. Meths. Biomed. Eng.*, 30:180–203, 2014.

[68] X. Yang. Error analysis of stabilized semi-implicit method of Allen-Cahn equation. *Disc. Conti. Dyn. Sys. -B*, 11:1057–1070, 2009.

[69] X. Yang. Linear, first and second-order, unconditionally energy satble numerical schemes for the phase field model of homopolymer blends. *J. Comput. Phys.*, 327:294–316, 2016.

[70] X. Yang. Numerical approximations for the Cahn-Hilliard phase field model of the binary fluid-surfactant system. *DOI: 10.1007/s10915-017-0508-6, in press, J. Sci. Comput*, 2017.

[71] X. Yang, Z. Cui, M. G. Forest, Q. Wang, and J. Shen. Dimensional robustness & instability of sheared, semi-dilute, nano-rod dispersions. *SIAM Multi. Model. Simul.*, 7:622–654, 2008.

[72] X. Yang, J. J. Feng, C. Liu, and J. Shen. Numerical simulations of jet pinching-off and drop formation using an energetic variational phase-field method. *J. Comput. Phys.*, 218:417–428, 2006.

[73] X. Yang, M. G. Forest, H. Li, C. Liu, J. Shen, and Q. Wang. Modeling and simulations of drop pinch-off from liquid crystal filaments and the leaky liquid crystal faucet immsersed in viscous fluids. *J. Comput. Phys.*, 236:1–14, 2013.

[74] X. Yang, M. G. Forest, C. Liu, and J. Shen. Shear cell rupture of nematic droplets in viscous fluids. *J. Non-Newtonian Fluid Mech.*, 166:487–499, 2011.

[75] X. Yang, M. G. Forest, W. Mullins, and Q. Wang. Dynamic defect morphology and hydrodynamics of sheared nematic polymers in two space dimensions. *J. Rheology*, 53:589–615, 2009.

[76] X. Yang, M. G. Forest, W. Mullins, and Q. Wang. Quench sensitivity to defects and shear banding in nematic polymer film flows. *J. Non-Newtonian Fluid Mech.*, 159:115–129, 2009.

[77] X. Yang, M. G. Forest, W. Mullins, and Q. Wang. 2-d lid-driven cavity flow of nematic polymers: an unsteady sea of defects. *Soft Matter*, 6:1138–1156, 2010.

[78] X. Yang and L. Ju. Efficient linear schemes with unconditionally energy stability for the phase field elsatic bending energy model. *Comput. Methods Appl. Mech. Engrg.*, 315:691–712, 2017.

[79] X. Yang and L. Ju. Linear and unconditionally energy stable schemes for the binary fluid-surfactant phase field model. *Comput. Methods Appl. Mech. Engrg.*, 318:1005–1029, 2017.

[80] X. Yang and H. Yu. Linear, second order and unconditionally energy stable schemes for a phase-field moving contact line model. *arXiv:1703.01311*, 2017.

[81] X. Yang, J. Zhao, and Q. Wang. Numerical approximations for the molecular beam epitaxial growth model based on the invariant energy quadratization method. *J. Comput. Phys.*, 333:104–127, 2017.

[82] X. Yang, J. Zhao, Q. Wang, and J. Shen. Numerical approximations for a three components Cahn–Hilliard phase-field model based on the invariant energy quadratization method. *M3AS: Mathematical Models and Methods in Applied Sciences*, 27:1993–2030, 2017.

[83] H. Yu and X. Yang. Numerical approximations for a phase-field moving contact line model with variable densities and viscosities. *J. Comput. Phys.*, 35:665–686, 2017.

[84] P. Yue, J. J. Feng, C. Liu, and J. Shen. A diffuse interface method for simulating two phase flows of complex fluids. *J. Fluid Mech.*, 515:293–317, 2004.

[85] J. Zhao, Q. Wang, and X. Yang. Numerical approximations to a new phase field model for immiscible mixtures of nematic liquid crystals and viscous fluids. *Comput. Meth. Appl. Mech. Eng.*, 310:77–97, 2016.

[86] J. Zhao, Q. Wang, and X. Yang. Numerical approximations for a phase field dendritic crystal growth model based on the invariant energy quadratization approach. *Inter. J. Num. Meth. Engrg.*, 110:279–300, 2017.

[87] J. Zhao, X. Yang, Y. Gong, and Q. Wang. A novel linear second order unconditionally energy stable scheme for a hydrodynamic Q-tensor model of liquid crystals. *Comput. Meth. Appl. Mech. Eng.*, 318:803–825, 2017.

[88] J. Zhao, X. Yang, J. Li, and Q. Wang. Energy stable numerical schemes for a hydrodynamic model of nematic liquid crystals. *SIAM. J. Sci. Comput.*, 38:A3264–A3290, 2016.

[89] J. Zhao, X. Yang, J. Shen, and Q. Wang. A decoupled energy stable scheme for a hydrodynamic phase field model of mixtures of nematic liquid crystals and viscous fluids. *J. Comput. Phys.*, 305:539–556, 2016.

[90] C. Zhou, P. Yue, and J. J. Feng. Dynamic simulation of droplet interaction and self-assembly in a nematic liquid crystal. *Langmuir*, 24:3099–3110, 2008.